

DTIC FILE COPY

UNCLASSIFIED

1

AD-A213 452

DTIC
ELECTE
OCT 17 1989
S D^{as} D

FINAL TECHNICAL REPORT SBIR PH I

OPTIMUM NAVIGATION STUDY

Contract # F04704-85-C-0166
85 Sept. 30-86 Mar. 31

Dr. Barry Mons
American Technical Services
Solana Beach, CA 92075

April 1987

Approved for Public Release; Distribution Unlimited

UNCLASSIFIED

89 10 17 015

REPORT DOCUMENTATION PAGE

Form Approved
OMB No. 0704-0188

1a. REPORT SECURITY CLASSIFICATION UNCLASSIFIED			1b. RESTRICTIVE MARKINGS None		
2a. SECURITY CLASSIFICATION AUTHORITY			3. DISTRIBUTION / AVAILABILITY OF REPORT Statement A: Approved for public release; distribution is unlimited.		
2b. DECLASSIFICATION / DOWNGRADING SCHEDULE					
4. PERFORMING ORGANIZATION REPORT NUMBER(S)			5. MONITORING ORGANIZATION REPORT NUMBER(S) BMO-TR-87-24		
6a. NAME OF PERFORMING ORGANIZATION American Technical Services		6b. OFFICE SYMBOL (If applicable)		7a. NAME OF MONITORING ORGANIZATION HQ Ballistic Missile Office/MYEG	
6c. ADDRESS (City, State, and ZIP Code) 245 Loma Corta Drive Solana Beach CA 92075			7b. ADDRESS (City, State, and ZIP Code) Norton AFB CA 92409-6468		
8a. NAME OF FUNDING / SPONSORING ORGANIZATION		8b. OFFICE SYMBOL (If applicable)		9. PROCUREMENT INSTRUMENT IDENTIFICATION NUMBER F04704-85-C-0166	
8c. ADDRESS (City, State, and ZIP Code)			10. SOURCE OF FUNDING NUMBERS		
			PROGRAM ELEMENT NO. 65502F	PROJECT NO. SBIR FY86	TASK NO. WORK UNIT ACCESSION NO.
11. TITLE (Include Security Classification) Optimum Navigation Study (U)					
12. PERSONAL AUTHOR(S) Mons, Barry					
13a. TYPE OF REPORT Final, Phase I		13b. TIME COVERED FROM 850930 TO 860331		14. DATE OF REPORT (Year, Month, Day) 860331	
15. PAGE COUNT					
16. SUPPLEMENTARY NOTATION					
17. COSATI CODES			18. SUBJECT TERMS (Continue on reverse if necessary and identify by block number)		
FIELD	GROUP	SUB-GROUP			
17	07		Navigation, optimum, modern control; Kalman Filtering, Miss Distance, Midcourse and Terminal Guidance Laws		
19. ABSTRACT (Continue on reverse if necessary and identify by block number)					
<p>Current and future defensive missile systems have to counter threats that operate at great speeds at high altitudes and that employ increasingly more sophisticated self-screening countermeasures. To counter such a threat, it is essential that the United States exploit both current and future missile systems to their maximum potential by developing optimum midcourse and terminal guidance laws that will minimize terminal miss distance and require a minimum amount of energy. The optimum navigation study presented will develop the optimum navigation laws for RVs equipped with terminal homing capability and will demonstrate the performance of such an RV in terms of actual miss distance.</p>					
20. DISTRIBUTION / AVAILABILITY OF ABSTRACT <input checked="" type="checkbox"/> UNCLASSIFIED/UNLIMITED <input type="checkbox"/> SAME AS RPT <input type="checkbox"/> DTIC USERS			21. ABSTRACT SECURITY CLASSIFICATION UNCLASSIFIED		
22a. NAME OF RESPONSIBLE INDIVIDUAL Ronald Lee, Lt. USAF			22b. TELEPHONE (Include Area Code) 714-382-7501 (AV-876)		22c. OFFICE SYMBOL HQ BMO/MYEG

INITIAL DISTRIBUTION LIST

Department of the Air Force
Headquarters Ballistic Missile Office/MYEG
Norton Air Force Base, CA 92409-6468

1 copy

Accession For	
NTIS CRA&I	<input checked="checked" type="checkbox"/>
DTIC TAB	<input type="checkbox"/>
Unannounced	<input type="checkbox"/>
Justification	
By	
Distribution /	
Availability Codes	
Dist	Avail and/or Special
A-1	

ACKNOWLEDGEMENT

The author wishes to acknowledge the contribution of Lynne Mons, his wife and secretary, without whose assistance this report could not have been published.

TABLE OF CONTENTS

Section	Page
Table of Contents	i
List of Figures	ii
List of Tables	iii
 Preface	 1
 1.0 Introduction	 2
 2.0 Optimal Midcourse Navigation Law Development	 5
2.1 Introduction	5
2.2 Midcourse Navigation Law Formulation	5
2.3 Quasi-Analytical Solution	7
2.4 Linear-Quadratic Solution	13
2.5 Midcourse Navigation Law Evaluation	19
 3.0 Optimal Terminal Navigation Law Development	 23
3.1 Introduction	23
3.2 Terminal Navigation Law Formulation	23
3.3 Optimal control Formulation	24
3.4 Optimal Control Solution	25
3.5 Time-to-go and Target Acceleration	29
3.6 Radome Boresight Errors	30
3.7 Terminal Navigation Law Evaluation	37
3.8 Navigation Law Implementation	38
 4.0 Conclusions	 42
 Bibliography	 43
 List of Symbols and Abbreviations	 44
 Index	 45

LIST OF FIGURES

Figure		Page
1	Miss-Distance Sensitivity with a Step Displacement in Handover-to-Terminal Point versus Time-to-go.	20
2	Guidance Error Sensitivity to Update Accuracy	20
3	Wave Mechanism in Hollow Dielectric Shell	30
4	Sensor/Missile/Target Angular Relationships	31
5	Missile Guidance System Showing Boresight Error Feedback	32
6	Illustration of Relationship between Boresight Error Characteristics and Oscillation Amplitude	34
7	Miss due to Transient Type Cause for a Sampling Rate of 40 cps	40
8	Miss due to Noise Causes for a Sampling Rate of 40 cps	41

LIST OF TABLES

Table	Page
1 Seeker Field of View Requirements	22

INITIAL DISTRIBUTION LIST

Department of the Air Force
Headquarters Ballistic Missile Office/MYEG
Norton Air Force Base, CA 92409-6468

1 copy

PREFACE

This report is the result of a Phase I SBIR feasibility study into optimum navigation for an extended range intercept missile. The problem is to obtain an optimal guidance law for both the midcourse and the terminal guidance phase, where the different constraints for the two phases are satisfied. Direct application of the optimal guidance theory will result in a nonlinear two-point boundary value problem, and the complications due to the constraints make an analytical development of a guidance and control law usually impossible.

The conventional approach to this problem is to depend on iterative methods in the implementation of the optimum guidance law that satisfies the constraints. In this report, a computational scheme has been developed that does not require iteration, and that is generally implementable as an on-board, real-time guidance law. In this scheme the nonlinear equations are replaced by first order linear approximations, with a set of corrections added to account for the nonlinearities. These nonlinearities are made to be known functions of time by using the information from the inertial reference unit (IRU).

Two low-order examples have been included in the report, in order to demonstrate the computational technique. The navigation law performance and the sensitivity to errors and updates for both the midcourse and the terminal guidance modes have been evaluated using ATS's adjoint simulation.

1.0 INTRODUCTION

The guidance problem for an extended range intercept missile is to obtain an optimal guidance law for both midcourse and terminal guidance phases. These missiles typically include command update, inertial midcourse guidance and active or semiactive terminal guidance.

The function of the midcourse guidance law is to minimize energy loss and bring the heading error to zero at handover. Handover is the change from midcourse to terminal guidance and occurs following target acquisition by the missile seeker. A midcourse guidance phase by itself is generally not fast enough to consistently achieve a miss distance that is within the lethal radius of the warhead and a terminal guidance mode is necessary to achieve the required miss-distance results. The use of midcourse guidance followed by a relatively short period of terminal homing offers a significant improvement in firepower and missile intercept coverage at the expense of the addition of inertial sensors and their initialization and data links. The success or failure of the terminal guidance phase is affected by several factors. Seeker acquisition plays an important role at the desired time of handover. The heading error at handover is an essential variable, affecting the terminal miss-distance, depending on the missile-to-target range, missile speed, autopilot and control loop dynamic response, guidance filter time constants and possible radome boresight error coupling. As the missile approaches intercept, speed and maneuverability can become critical if a crossing and/or maneuvering target has to be intercepted, since the interceptor requires from three to five times the maneuver capability of the target. Other factors affecting terminal guidance accuracy and miss-distance results include target glint and severe fades in the target-reflected signal at critical times prior to intercept.

A combined guidance law for the midcourse and terminal guidance phase is developed in this report using optimal control techniques. However, direct application of the optimal control theory will result in a nonlinear two-point boundary value problem. The problem can be further complicated by lift, thrust and control constraints forced by structural and angle-of-attack limits and the direct analytical development of a guidance and control law is usually out of reach.

Some effective, sophisticated, numerical optimization methods have been programmed, often in double precision arithmetic, that construct a single optimum guided trajectory in 10 to 20 minutes. These techniques will not be applicable for many years to real-time control of missiles with compact, light-weight navigation and control computers. Attempts have been made to pre-compute one nominal optimum trajectory and then fit thrust angle regimes in-flight to the pre-computed optimal trajectory. This kind of implicit solution is useful if the perturbations in the initial conditions and perturbations in the thrust level are sufficiently low. But if the mission requires many different powered

flight maneuvers, such as with maneuvering re-entry vehicles, the solution based on pre-computer reference trajectories becomes very unattractive.

In this report two more easily implementable computational schemes have been developed that allow real-time on-board implementation. The first uses a quasi-analytical approach that provides a solution process without the traditional dependence on iterative numerical methods, and the second takes advantage of the knowledge of the value of the nonlinear term, obtained from the available inertial reference unit.

Since the intercept missiles have to counter a wide variety of targets under extreme operating conditions, it is required that the optimal navigation law is (1) independent of standard conditions and (2) nominal trajectories and (3) transitions smoothly from midcourse to terminal navigation.

The first two requirements can be met by seeking the solution of the actual differential equations of motion, while the third requirement has been met by letting the solution be subject to the appropriate boundary conditions at terminal handover. A requirement for minimum energy during flight can be included in a performance index that defines the parameters or states to be minimized. Since the minimization of the desired parameters can often lead to conflicting strategies (i.e. minimum fuel and minimum time) the weighting terms will be employed in the performance index (or cost functional) to define the degree of minimization for each parameter. Ideally, the determination of the parameters to be minimized is a direct result of the mission requirements. In certain cases however, the translation of mission requirements to the performance index leads to unrealizable or non-unique navigation strategies. In that case, additional terms (secondary mission requirements) have to be added to the performance index. Care must be taken in selecting and weighing the additional performance criteria, such that the primary criteria are not significantly de-emphasized.

System/state constraints can be handled explicitly or implicitly by the optimal control formulation. In the vehicle control problem, these constraints may be factors, such as acceleration limits, seeker angle or rate limits, terminal constraints, such as zero miss-distance, terminal aspect angle, or other state constraints that may limit the performance of the system. If those constraints are included explicitly, the solutions lead to a two-point boundary value problem that can only be solved by iterative numerical techniques which are very sensitive to modeling and measurement error, making on-line real-time solutions with microprocessors difficult at best. For these reasons, explicit constraints are handled implicitly through the performance criterion by minimizing the constrained factors.

Two low order examples have been included in this report to demonstrate the computational schemes used to allow real-time implementation. Of those two, the quasi-analytical solution is the more general and powerful approach and although the tech-

nique may not be applicable for point-to-point guidance techniques, it warrants further research for application to intercept missile guidance techniques.

The navigation law performance and sensitivity to errors and updates have been evaluated using ATS's adjoint simulation for both the midcourse and terminal guidance modes.

2.0 OPTIMAL MIDCOURSE NAVIGATION LAW DEVELOPMENT

2.1 Introduction

As stated in Section 1.0, there are many considerations in developing the optimal navigation laws via optimal control theory. The criteria to be considered include complexity, ease of implementation, sensitivity to errors and updates, availability of measurements, ease of handover to terminal navigation for the midcourse navigation law, and minimum miss distance for the terminal navigation law. Navigation law performance and sensitivity to errors and updates have been evaluated for the BIM using ATS's adjoint simulation for both the midcourse and terminal navigation modes. For the terminal navigation mode the resulting miss is also a function of statistical disturbances, such as glint or angular scintillation noise, (which increases with decreasing range), effective receiver noise, (which decreases with decreasing range), and amplitude or range independent noise caused by the servo system and by amplitude fluctuations in the received signal. In addition, for a system such as the BIM, parasitic coupling with the vehicle's airframe caused by aberration of the electromagnetic energy as it passes through the cover protecting the terminal sensor, needs to be considered. This error typically depends on the vehicle's altitude and it couples the airframe dynamics to the terminal sensor measurements, causing possible airframe instability. Because of the interest expressed in this error source during a visit to BMO, a brief analysis demonstrating the resulting feedback paths that can cause missile system instability has been included.

Historically, miss distance simulations for a system with statistical disturbances have employed tedious Monte Carlo techniques to obtain terminal miss-distance results. ATS has used its adjoint simulation to determine the effects of initial condition errors at handover and the effects of statistical disturbances on missile miss-distance performance. While Monte Carlo simulations require many runs to obtain statistically meaningful results, the adjoint technique of analysis is a proven statistical analysis tool that generates the rms miss-distance in only one run. The adjoint technique of analysis and the adjoint simulation used in this Phase I Study are described in Appendix A and B.

2.2 Midcourse Navigation Law Formulation

The development of the optimal midcourse navigation policy has been accomplished using the differential equations of motion of the vehicle in the navigation frame, that is used by the inertial platform and was transferred at launch to the inertial reference system, together with the handover to terminal navigation, which in turn is a function of the target location. If the target is a moving, non-cooperative target, this handover to terminal navigation point may have to be updated during its midcourse flight.

The derivations assume that the navigation takes place in an earth-centered inertial

cartesian coordinate reference frame.

The midcourse navigation problem is a two-point boundary value problem which consists of the vehicle's current position and velocity vectors

$$\begin{aligned} r(t_o) &= (x_o, y_o, z_o) \\ v(t_o) &= (\dot{x}_o, \dot{y}_o, \dot{z}_o) \end{aligned} \quad (1)$$

and the required position and velocity factors at handover

$$\begin{aligned} r(t_f) &= (x_f, y_f, z_f) \\ v(t_f) &= (\dot{x}_f, \dot{y}_f, \dot{z}_f) \end{aligned} \quad (2)$$

The requirement is then to find the thrust acceleration program for $t_o \leq t \leq t_f$ that drives the vehicle from its initial boundary condition to the terminal boundary condition. The differential equations of motion of a missile are

$$\ddot{\mathbf{r}} = \mathbf{g} + \mathbf{a} \quad (3)$$

or in component form

$$\begin{aligned} \ddot{x} &= g_x + a_x \\ \ddot{y} &= g_y + a_y \\ \ddot{z} &= g_z + a_z \end{aligned} \quad (4)$$

If the gravity field is assumed to be spherical, the above equations are non-linear, i.e.

$$\begin{aligned} \ddot{x} &= -\frac{\mu x}{(x^2 + y^2 + z^2)^{\frac{3}{2}}} + a_x \\ \ddot{y} &= -\frac{\mu y}{(x^2 + y^2 + z^2)^{\frac{3}{2}}} + a_y \\ \ddot{z} &= -\frac{\mu z}{(x^2 + y^2 + z^2)^{\frac{3}{2}}} + a_z \end{aligned} \quad (5)$$

The difficulty in obtaining an optimal control solution to the above dynamic equations is the presence of the non-linear terms. Only rarely is it feasible to solve the resulting two-point boundary value differential equation for a non-linear system, and the development of "exact" guidance and control schemes for non-linear systems is usually out of reach. In this report, however, we will obtain the optimal control solution using:

1. a quasi-analytical approach obtained from a straightforward expansion of perturbation methods, which provides a solution process without the traditional dependence on iterative numerical methods, and

2. a guidance and control scheme where the guidance computer generates the non-linear terms as a function of missile position, and allows the optimal control problem to be treated as a linear-quadratic system.

For both methods the performance criterion used is minimum mean-squared error. There are a number of reasons for this choice. As is always true in optimum linear theory - whether optimum filtering, optimum control or other special case - the quadratic error criterion, of all reasonable criteria, leads to the most tractable formulation of the optimum design problem. In addition, a criterion is desired which is universally applicable to all forms of input signals. No other such criterion has demonstrated to give superior results over a broad range of problems.

2.3 Quasi-Analytical Solution

The non-linear equations from (5) can be written in the state variable form as follows:

$$\begin{aligned}
 \dot{x}_1 &= x_2 \\
 \dot{x}_2 &= -\frac{\mu x_1}{(x_1^2 + x_3^2 + x_5^2)^{\frac{3}{2}}} + u_x \\
 \dot{x}_3 &= x_4 \\
 \dot{x}_4 &= -\frac{\mu x_3}{(x_1^2 + x_3^2 + x_5^2)^{\frac{3}{2}}} + u_y \\
 \dot{x}_5 &= x_6 \\
 \dot{x}_6 &= -\frac{\mu x_5}{(x_1^2 + x_3^2 + x_5^2)^{\frac{3}{2}}} + u_z
 \end{aligned} \tag{6}$$

or in matrix notation

$$\dot{x} = Ax + Bu + f(x) \tag{7}$$

where

$$A = \begin{pmatrix} 0 & 1 & 0 & 0 & 0 & 0 \\ 0 & 0 & 0 & 0 & 0 & 0 \\ 0 & 0 & 0 & 1 & 0 & 0 \\ 0 & 0 & 0 & 0 & 0 & 0 \\ 0 & 0 & 0 & 0 & 0 & 1 \\ 0 & 0 & 0 & 0 & 0 & 0 \end{pmatrix}; \quad B = \begin{pmatrix} 0 & 0 & 0 \\ 1 & 0 & 0 \\ 0 & 0 & 0 \\ 0 & 1 & 0 \\ 0 & 0 & 0 \\ 0 & 0 & 1 \end{pmatrix} \tag{8}$$

and

$$f(x) = \begin{pmatrix} 0 \\ -\mu x_1 / (x_1^2 + x_3^2 + x_5^2)^{\frac{3}{2}} \\ 0 \\ -\mu x_3 / (x_1^2 + x_3^2 + x_5^2)^{\frac{3}{2}} \\ 0 \\ -\mu x_5 / (x_1^2 + x_3^2 + x_5^2)^{\frac{3}{2}} \end{pmatrix} \tag{9}$$

We seek the optimal control trajectory that will minimize the quadratic performance index

$$J = \frac{1}{2} x^T S x|_{t=t_f} + \frac{1}{2} \int_{t_0}^{t_f} (x^T Q x + u^T R u) dt \quad (10)$$

where R and S are positive definite weighting matrices and Q a symmetric positive semi-definite weighting matrix in which $Q = 0$ is not excluded. The Hamiltonian formed from the system equation (7) and the integrand of equation (10) is given by

$$H = \frac{1}{2} (x^T Q x + u^T R u) + \lambda^T (A x + B u + f(x)) \quad (11)$$

where the costates λ are a set of as yet undetermined Lagrange multipliers. Pontryagin's necessary conditions for determining the optimal control obtained by operating on the Hamiltonian, yield the equations

$$\dot{x} = H_\lambda = A x + B u + f(x) \quad (12)$$

$$\dot{\lambda} = -H_x = -Q x - A^T \lambda - \left(\frac{\partial f(x)}{\partial x} \right)^T \lambda \quad (13)$$

$$0 = H_u = R u + B^T \lambda \quad (14)$$

with the boundary condition $\lambda(t_f) = S x(t_f)$.

Solving equation (14) for u results in $u = -R^{-1} B^T \lambda$ and substituting this into equation (12) reduces the optimal control problem to two-coupled first order, non-linear, ordinary differential equations, i.e.

$$\dot{x} = A x - B R^{-1} B^T \lambda + f(x) \quad (15)$$

$$\dot{\lambda} = -Q x - A^T \lambda - \left(\frac{\partial f(x)}{\partial x} \right)^T \lambda \quad (16)$$

Combining the unknowns x and λ into a single augmented state/costate vector z , the optimal control problem can be restated as

$$\dot{z} = F z + \epsilon \rho \quad (17)$$

where

$$z = (\lambda^T x^T)^T \quad (18)$$

$$F = \begin{pmatrix} A & -B R^{-1} B^T \\ -Q & -A^T \end{pmatrix} \quad (19)$$

$$\rho = \begin{pmatrix} f(x) \\ -\left(\frac{\partial f(x)}{\partial x} \right)^T \lambda \end{pmatrix} \quad (20)$$

with boundary conditions $x(t_0) = x(0)$ and $\lambda(t_f) = S x(t_f)$ and where the dimensionless parameter ϵ is a bookkeeping term to keep track of the order of the nonlinear terms.

After solving the two-point boundary value problem given by equation (17), the state trajectories and optimal control can be determined. However, because of the presence of the non-linear terms, the system governed by equation (17) is analytically intractable. Although there are many iterative techniques available for solving such non-linear systems, they are not suitable for on-board implementation. We will therefore develop a quasi-analytical technique that will circumvent the iterative techniques.

Assume that the solution to equation (17) may be represented by a power series in terms of a small parameter ϵ by

$$z(t) = z_0(t) + \epsilon z_1(t) + \epsilon^2 z_2(t) + \epsilon^3 z_3(t) + \dots \quad (21)$$

For small nonlinearities the series will converge, while the accuracy will improve as the nonlinearities approach zero. Similarly, for a convergent series, the accuracy can be improved by using more terms, in fact as the number of terms in the series approaches infinity, the solution given by equation (21) will be exact. Substituting equation (21) into (17) we can write

$$\dot{z}_0 + \epsilon \dot{z}_1 + \epsilon^2 \dot{z}_2 + \epsilon^3(0) = Fz_0 + \epsilon Fz_1 + \epsilon^2 Fz_2 + \epsilon \rho_1(z_0) + \epsilon^2 \rho_2(z_0, z_1) + \epsilon^3(0) \quad (22)$$

where the nonlinear terms have been expanded in a similar power series and the dependence of the nonlinear term on the z variable is indicated by z_i . Equating terms with equivalent powers of ϵ results in the following set of differential equations.

$$\dot{z}_0 = Fz_0 \quad (23)$$

$$\dot{z}_1 = Fz_1 + \rho_1(z_0) \quad (24)$$

$$\dot{z}_2 = Fz_2 + \rho_2(z_0, z_1) \quad (25)$$

with the boundary conditions

$$z_0(t_0) = \begin{pmatrix} x(t_0) \\ \lambda_0(t_0) \end{pmatrix}, z_0(t_f) = \begin{pmatrix} x(t_f) \\ \lambda_0(t_f) \end{pmatrix}$$

and

$$z_i(t_0) = \begin{pmatrix} 0 \\ \lambda_i(t_0) \end{pmatrix}, z_i(t_f) = \begin{pmatrix} 0 \\ 0 \end{pmatrix} \quad i = 1, 2, 3, \dots$$

and where the final conditions of the states and costates are related to each other through the boundary condition $\lambda_i(t_f) = Sz_i(t_f)$.

Thus, we obtained a strictly linear first order approximation (equation (22)) to the original nonlinear problem and a series of correction terms (equations (23) through (25)) to account for the effects of the nonlinearities, while the nonlinear term in the correction terms is independent of the z variable of that particular differential equation.

Furthermore, the order can simply be extended to achieve the degree of accuracy required for a specific problem.

The solution of the system of equations given by equations (23) through (25) is given by

$$z_i(t) = e^{F(t)} z_i(0) + \int_0^t e^{F(t-\tau)} \rho_i(\tau) d\tau \quad i = 0, 1, 2, \dots \quad (28)$$

or equivalently

$$z_i(t) = \Phi(t) z_i(0) + \int_0^t \Phi(t-\tau) \rho_i(\tau) d\tau \quad i = 0, 1, 2, \dots \quad (29)$$

with $\rho_o(\tau) = 0$ and where without loss of generality t_o has been replaced by 0. In shorthand notation we can rewrite (28) as

$$z_i(t) = \Phi(t) z_i(0) + \Psi_i(t) \rho_i \quad (30)$$

However, at this point the initial costates $\lambda_i(t_o)$ thus $z_i(t_o)$ are as yet undetermined. If we expand the state transition matrix into

$$\Phi_i(t) = \begin{pmatrix} \Phi_{11}(t) & \Phi_{12}(t) \\ \Phi_{21}(t) & \Phi_{22}(t) \end{pmatrix}$$

and the last term of equation (30) into

$$\Psi_i(t) \rho_i = \begin{pmatrix} \Psi_{1i}(t) \\ \Psi_{2i}(t) \end{pmatrix}$$

then on recalling the boundary conditions of equation (20) we can write at $t = t_f$

$$\begin{aligned} x_i(t_f) &= \Phi_{11}(t_f) x_i(0) + \Phi_{12}(t_f) \lambda_i(0) + \Psi_{1i}(t_f) \\ S x_i(t_f) &= \Phi_{21}(t_f) x_i(0) + \Phi_{22}(t_f) \lambda_i(0) + \Psi_{2i}(t_f) \end{aligned} \quad (33)$$

in which $\lambda_i(0)$ is the only unknown. Multiplying equation (33) by the positive definite matrix S and subtracting the resulting equation from (34) results in

$$[\Phi_{22}(t_f) - S\Phi_{12}(t_f)] \lambda_i(0) = [S\Phi_{11}(t_f) - \Phi_{21}(t_f)] x_i(0) + S\Psi_{1i}(t_f) - \Psi_{2i}(t_f) \quad (34)$$

from which the original costates are:

$$\lambda_i(0) = [\Phi_{22}(t_f) - S\Phi_{12}(t_f)]^{-1} [(S\Phi_{11}(t_f) - \Phi_{21}(t_f)) x_i(0) + S\Psi_{1i}(t_f) - \Psi_{2i}(t_f)] \quad (35)$$

Now with all initial conditions known, equation (29) can be used to obtain the optimal control at any time in the interval $0 \leq t \leq t_f$. The original nonlinear control problem

has thus been expanded to a set of non-homogeneous, linear, optimal control problems that may be solved sequentially.

The effectiveness of the quasi-analytical method is demonstrated with an example of a system with both quadratic and cubic nonlinear terms. The system is given by

$$\dot{x}_1 = x_2 \quad (36)$$

$$\dot{x}_2 = -x_1 - .1x_2 + u + .1(ux_1 - .5x_1^3) \quad (37)$$

or

$$\dot{x} = \begin{pmatrix} 0 & 1 \\ -1 & -.1 \end{pmatrix} x + \begin{pmatrix} 0 \\ .1 \end{pmatrix} u + \begin{pmatrix} 0 \\ .1 \end{pmatrix} (ux_1 - .5x_1^3) \quad (38)$$

or in short

$$\dot{x} = Ax + bu + cf(x, u) \quad (39)$$

The objective is to determine the optimal controls that will drive x_1 from one to zero in a 2 second interval. The corresponding performance criterion is

$$J = \frac{1}{2}x^T Sx + \frac{1}{2} \int_0^2 u^2 dt \quad (40)$$

with $s_1 = s_2 = 100$. The Hamiltonian is given by $H = \frac{1}{2}u^2 + \lambda^T(Ax + bu + cf(x, u))$ and Pontryagin's necessary conditions for determining the optimal controls are

$$H_\lambda = \dot{x} = Ax + bu + cf(x, u) \quad (41)$$

$$-H_x = \dot{\lambda} = -A^T\lambda - \frac{\partial f}{\partial x}c^T\lambda \quad (42)$$

$$H_u = 0 = u + b^T\lambda + \frac{\partial f}{\partial u}c^T\lambda \quad (43)$$

or

$$u = -b^T\lambda - \frac{\partial f}{\partial u}c^T\lambda \quad (44)$$

Substituting the optimal control into the differential equations results in:

$$\dot{x} = Ax - bb^T\lambda - b\frac{\partial f}{\partial u}c^T\lambda + cf(x, u) \quad (45)$$

$$\dot{\lambda} = -A^T\lambda - c\frac{\partial f}{\partial x}c^T\lambda$$

Combining the unknowns x and λ into a single augmented state/costate vector z , the optimal control problem can be restated as

$$\dot{z} = Fz + \epsilon\rho \quad (46)$$

where

$$z = (\lambda^T x^T)^T \quad (47)$$

$$F = \begin{pmatrix} 0 & 1 & 0 & 0 \\ -1 & -.1 & 0 & -1 \\ 0 & 0 & 0 & 1 \\ 0 & 0 & -1 & -.1 \end{pmatrix} \quad (48)$$

and

$$\epsilon \rho = .1 \begin{pmatrix} 0 \\ -x_1 \lambda_2 + (u x_1 - .5 x_1^3) \\ 0 \\ -(u - 1.5 x_1^2) \lambda_2 \end{pmatrix} \quad (49)$$

The effectiveness of the optimal control approximation was evaluated by integrating equation (46) numerically using a fourth order Runge Kutta routine and examining the terminal boundary condition errors of the numerically integrated solution with those of a second order expansion.

The second order expansion yields a final condition error of $x(t) = -.000321$ from the integrated equation of motion. Although not exactly zero, the error is less than 0.035%. By comparison, the linearized optimal control, obtained by dropping the nonlinear terms produces $x(t_f) = -.0382$, or an error of slightly less than 4.0%. Thus the perturbation method reduced the error by more than two orders of magnitude for a second order expansion, demonstrating the effectiveness of the method.

The secret to the success of this powerful method lies of course in the selection of a convergent series for the assumed solution. This will occur automatically if the selection of z_0 is close to the actual solution, ensuring that the correction terms will be small. Selection of such an initial solution is illustrated by an example of determining the near-circular orbit period of an earth satellite. The coupled radial and tangential force equations for such a system are given by

$$\ddot{r} - r\dot{\psi}^2 = -\frac{\mu}{r^2} \quad (50)$$

and

$$r\ddot{\psi} + 2\dot{r}\dot{\psi} = 0 \quad (51)$$

Since this latter equation can be written as $\frac{1}{r} \frac{d}{dt}(r^2 \dot{\psi}) = 0$, we can write $r^2 \dot{\psi} = h$ where we defined:

r as the distance from the center of the earth to the satellite,

ψ as the angle between r and an arbitrary reference,

μ as a constant defining the specific gravitational force,

h as the constant specific angular momentum of the orbit.

Eliminating $\dot{\psi}$ from the above equations results in the non-linear system differential equation

$$\ddot{r} - \frac{h^2}{r^3} = -\frac{\mu}{r^2} \quad (52)$$

for which we have to assume a solution. The geometry of the problem suggests a solution of the form

$$r = R + \delta_R \cos \psi \quad (53)$$

where $\psi = \omega t$ with R and δ_R as constants.

Substituting this expression in the nonlinear system equation results in

$$-\omega^2 \delta_R \cos \psi - \frac{h^2}{R^3} \left(1 + \frac{3\delta_R}{R} \cos \psi\right)^{-3} = -\frac{\mu}{R^2} \left(1 + \frac{\delta_R}{R} \cos \psi\right)^{-2} \quad (54)$$

The assumption of a near-circular orbit implies that $\delta_R/R \ll 1$ and the above equation can be approximated by the following first-order expansions

$$-\omega^2 \delta_R \cos \psi - \frac{h^2}{R^3} \left(1 - \frac{3\delta_R}{R} \cos \psi\right) = -\frac{\mu}{R^2} \left(1 - \frac{2\delta_R}{R} \cos \psi\right) \quad (55)$$

Equating terms with equivalent powers results in the following set of equations

$$R = \frac{h^2}{\mu} \quad (56)$$

$$\omega^2 = \frac{3h^2}{R^4} - \frac{2\mu}{R^3} \quad (57)$$

Solution of these two equations for the orbit of period T is now easy and yields

$$T = \frac{2\pi}{\omega} = 2\pi \frac{h^3}{\mu^2} \quad (58)$$

which compares favorably with the exact result (where orbit eccentricity = δ_R/R) of

$$T_{exact} = 2\pi \frac{h^3}{\mu^2} \left[1 - \left(\frac{\delta_R}{R}\right)^2\right]^{-\frac{3}{2}} \quad (59)$$

2.4 Linear-Quadratic Solution

In a missile system that is aware of its physical position with its Inertial Reference Unit (IRU), we have the option of calculating the actual value of the nonlinear terms such as gravity at each instant of time, and use that value to modify the required total optimal acceleration. This total optimal acceleration can be calculated using the linear-quadratic

approach as discussed below. Using the total acceleration concept we can rewrite the system equations (5) as:

$$\begin{aligned}
 \dot{x}_1 &= x_2 \\
 \dot{x}_2 &= \frac{-\mu x_1}{(x_1^2 + x_3^2 + x_5^2)^{3/2}} + a_x = u_1 \\
 \dot{x}_3 &= x_4 \\
 \dot{x}_4 &= \frac{-\mu x_3}{(x_1^2 + x_3^2 + x_5^2)^{3/2}} + a_y = u_2 \\
 \dot{x}_5 &= x_6 \\
 \dot{x}_6 &= \frac{-\mu x_5}{(x_1^2 + x_3^2 + x_5^2)^{3/2}} + a_z = u_3
 \end{aligned} \tag{60}$$

or in matrix notation

$$\dot{x} = Ax + Bu \tag{61}$$

where

$$A = \begin{pmatrix} 0 & 1 & 0 & 0 & 0 & 0 \\ 0 & 0 & 0 & 0 & 0 & 0 \\ 0 & 0 & 0 & 1 & 0 & 0 \\ 0 & 0 & 0 & 0 & 0 & 0 \\ 0 & 0 & 0 & 0 & 0 & 1 \\ 0 & 0 & 0 & 0 & 0 & 0 \end{pmatrix} \text{ and } B = \begin{pmatrix} 0 & 0 & 0 \\ 1 & 0 & 0 \\ 0 & 0 & 0 \\ 0 & 1 & 0 \\ 0 & 0 & 0 \\ 0 & 0 & 1 \end{pmatrix} \tag{62}$$

We seek the optimal control that will minimize the quadratic performance index

$$J = 1/2 x^T(t_f) S x(t_f) + 1/2 \int_{t_0}^{t_f} (u^T R u) dt \tag{63}$$

where

$$S = \begin{pmatrix} s_1 & 0 & 0 & 0 & 0 & 0 \\ 0 & s_2 & 0 & 0 & 0 & 0 \\ 0 & 0 & s_3 & 0 & 0 & 0 \\ 0 & 0 & 0 & s_4 & 0 & 0 \\ 0 & 0 & 0 & 0 & s_5 & 0 \\ 0 & 0 & 0 & 0 & 0 & s_6 \end{pmatrix} \text{ and } R = \begin{pmatrix} r_1 & 0 & 0 \\ 0 & r_2 & 0 \\ 0 & 0 & r_3 \end{pmatrix} \tag{64}$$

are positive definite, diagonal weighting matrices.

The Hamiltonian formed from the system equations (61) and the integrand of the equation (63) is given by

$$H = 1/2 u^T R u + \lambda^T (Ax + Bu) \tag{65}$$

where λ is the costate vector of the Lagrange multipliers. Pontryagin's necessary conditions for determining the optimal control obtained by operating on the Hamiltonian

yield the equations

$$\dot{x} = H_x = Ax + Bu \quad (66)$$

$$\dot{\lambda} = -H_\lambda = -A^T \lambda \quad (67)$$

$$0 = H_u = Ru + B^T \lambda \quad (68)$$

with the boundary conditions $x(t_0) = x(0)$ and $\lambda(t_f) = Sx(t_f)$. Solving equation (68) for u results in $u = -R^{-1}B^T \lambda$ and substitution in equation (66) reduces the optimal control problem to two-coupled first order, ordinary differential equations, i.e.

$$\dot{x} = Ax - BR^{-1}B^T \lambda \quad (69)$$

$$\dot{\lambda} = -A^T \lambda \quad (70)$$

with boundary conditions $x(t_0) = x(0)$ and $\lambda(t_f) = Sx(t_f)$. Writing out the $\dot{\lambda}$ part we have

$$\begin{aligned} \dot{\lambda}_1 &= 0 \\ \dot{\lambda}_2 &= -\lambda_1 \\ \dot{\lambda}_3 &= 0 \\ \dot{\lambda}_4 &= -\lambda_3 \\ \dot{\lambda}_5 &= 0 \\ \dot{\lambda}_6 &= -\lambda_5 \end{aligned} \quad (71)$$

with boundary conditions $\lambda(t_f) = S_f x(t_f)$. Integration from t_f to t gives

$$\begin{aligned} \lambda_1(t) &= s_1 x_1(t_f) \\ \lambda_2(t) &= s_1 x_1(t_f)(t_f - t) + s_2 x_2(t_f) \\ \lambda_3(t) &= s_3 x_3(t_f) \\ \lambda_4(t) &= s_3 x_3(t_f)(t_f - t) + s_4 x_4(t_f) \\ \lambda_5(t) &= s_5 x_5(t_f) \\ \lambda_6(t) &= s_5 x_5(t_f)(t_f - t) + s_6 x_6(t_f) \end{aligned} \quad (72)$$

and the optimal control using $u^o = -R^{-1}B^T \lambda$ is then

$$\begin{aligned} u_1^o &= -\frac{s_1}{r_1} x_1(t_f)(t_f - t) - \frac{s_2}{r_1} x_2(t_f) \\ u_2^o &= -\frac{s_3}{r_2} x_3(t_f)(t_f - t) - \frac{s_4}{r_2} x_4(t_f) \\ u_3^o &= -\frac{s_5}{r_3} x_5(t_f)(t_f - t) - \frac{s_6}{r_3} x_6(t_f) \end{aligned} \quad (73)$$

or

$$u^o(t) = \begin{pmatrix} -\frac{s_1}{r_1} T & -\frac{s_2}{r_1} & 0 & 0 & 0 & 0 \\ 0 & 0 & -\frac{s_3}{r_2} T & -\frac{s_4}{r_2} & 0 & 0 \\ 0 & 0 & 0 & 0 & -\frac{s_5}{r_3} T & -\frac{s_6}{r_3} \end{pmatrix} x(t_f) \quad (74)$$

which gives us the optimal control in terms of the state variables at final time t_f and time-to-go, $T = (t_f - t)$.

To obtain the optimal control in terms of the current time t , we use the differential equations of motion which can be written as

$$\begin{aligned}
 \dot{x}_1 &= x_2 \\
 \dot{x}_2 &= -\frac{s_1}{r_1}x_1(t_f)(t_f - t) - \frac{s_2}{r_1}x_2(t_f) \\
 \dot{x}_3 &= x_4 \\
 \dot{x}_4 &= -\frac{s_3}{r_2}x_3(t_f)(t_f - t) - \frac{s_4}{r_2}x_4(t_f) \\
 \dot{x}_5 &= x_6 \\
 \dot{x}_6 &= -\frac{s_5}{r_3}x_5(t_f)(t_f - t) - \frac{s_6}{r_3}x_6(t_f)
 \end{aligned} \tag{75}$$

with boundary conditions at $t_0 = x(t_0)$. Integrating the above equation from t_0 to t_f results in

$$\begin{aligned}
 x_1(t_f) &= -\frac{s_1}{3r_1}x_1(t_f)T^3 - \frac{s_2}{2r_1}x_2(t_f)T^2 + x_2(o)T + x_1(o) \\
 x_2(t_f) &= -\frac{s_1}{2r_1}x_1(t_f)T^2 - \frac{s_2}{r_1}x_2(t_f)T + x_2(o) \\
 x_3(t_f) &= -\frac{s_3}{3r_2}x_3(t_f)T^3 - \frac{s_4}{2r_2}x_4(t_f)T^2 + x_4(o)T + x_3(o) \\
 x_4(t_f) &= -\frac{s_3}{2r_2}x_3(t_f)T^2 - \frac{s_4}{r_2}x_4(t_f)T + x_4(o) \\
 x_5(t_f) &= -\frac{s_5}{3r_3}x_5(t_f)T^3 - \frac{s_6}{2r_3}x_6(t_f)T^2 + x_6(o)T + x_5(o) \\
 x_6(t_f) &= -\frac{s_5}{2r_3}x_5(t_f)T^2 - \frac{s_6}{r_3}x_6(t_f)T + x_6(o)
 \end{aligned} \tag{76}$$

where $T = t_f - t$, or in matrix notation

$$\begin{pmatrix}
 1 + \frac{s_1}{3r_1}T^3 & \frac{s_2}{2r_1}T^2 & 0 & 0 & 0 & 0 \\
 \frac{s_1}{2r_1}T^2 & 1 + \frac{s_2}{r_1}T & 0 & 0 & 0 & 0 \\
 0 & 0 & 1 + \frac{s_3}{3r_2}T^3 & \frac{s_4}{2r_2}T^2 & 0 & 0 \\
 0 & 0 & \frac{s_3}{2r_2}T^2 & 1 + \frac{s_4}{r_2}T & 0 & 0 \\
 0 & 0 & 0 & 0 & 1 + \frac{s_5}{3r_3}T^3 & \frac{s_6}{2r_3}T^2 \\
 0 & 0 & 0 & 0 & \frac{s_5}{2r_3}T^2 & 1 + \frac{s_6}{r_3}T^2
 \end{pmatrix} x(t_f) \tag{77}$$

$$= \begin{pmatrix}
 1 & T & 0 & 0 & 0 & 0 \\
 0 & 1 & 0 & 0 & 0 & 0 \\
 0 & 0 & 1 & T & 0 & 0 \\
 0 & 0 & 0 & 1 & 0 & 0 \\
 0 & 0 & 0 & 0 & 1 & T \\
 0 & 0 & 0 & 0 & 0 & 1
 \end{pmatrix} x(t_0) \tag{78}$$

If the above equation can be solved for $x(t_f)$, then the result can be substituted into Eqn (74) to obtain the optimal control.

By rewriting the coefficient matrix of Eqn (78) as

$$\begin{pmatrix} 11 & 12 & 0 & 0 & 0 & 0 \\ 21 & 22 & 0 & 0 & 0 & 0 \\ 0 & 0 & 33 & 34 & 0 & 0 \\ 0 & 0 & 43 & 44 & 0 & 0 \\ 0 & 0 & 0 & 0 & 55 & 56 \\ 0 & 0 & 0 & 0 & 65 & 66 \end{pmatrix}$$

its inverse has been obtained and is

$$\begin{pmatrix} \frac{22}{A} & -\frac{12}{A} & 0 & 0 & 0 & 0 \\ -\frac{21}{A} & \frac{11}{A} & 0 & 0 & 0 & 0 \\ 0 & 0 & \frac{44}{B} & -\frac{34}{B} & 0 & 0 \\ 0 & 0 & -\frac{43}{B} & \frac{33}{B} & 0 & 0 \\ 0 & 0 & 0 & 0 & \frac{66}{C} & -\frac{56}{C} \\ 0 & 0 & 0 & 0 & -\frac{65}{C} & \frac{55}{C} \end{pmatrix}$$

where

$$A = 11x22 - 12x21$$

$$B = 33x44 - 34x43$$

$$C = 55x66 - 65x56$$

Post-multiplying Eqn (74) with Eqn (80) and the right hand side of Eqn (77) or Eqn (78), substituting the actual terms from the coefficient matrix, and letting the current time $t = t_0$, results in the continuous optimal feedback control terms

$$\begin{aligned} u_1^o(t) = & - \frac{6s_1T(s_2T + 2r_1)}{s_1s_2T^4 + 4r_1s_1T^3 + 12r_1s_2T + 12r_1^2}x_1(t) \\ & - 4 \frac{s_1s_2T^3 + 3s_1r_1T^2 + 3r_1s_2}{s_1s_2T^4 + 4r_1s_1T^3 + 12r_1s_2T + 12r_1^2}x_2(t) \\ u_2^o(t) = & - \frac{6s_3T(s_4T + 2r_2)}{s_3s_4T^4 + 4r_2s_3T^3 + 12r_2s_4T + 12r_2^2}x_2(t) \\ & - 4 \frac{s_3s_4T^3 + 3s_3r_2T^2 + 3r_2s_4}{s_3s_4T^4 + 4r_2s_3T^3 + 12r_2s_4T + 12r_2^2}x_4(t) \\ u_3^o(t) = & - \frac{6s_5T(s_6T + 2r_3)}{s_5s_6T^4 + 4r_3s_5T^3 + 12r_3s_6T + 12r_3^2}x_5(t) \\ & - 4 \frac{s_5s_6T^3 + 3s_5r_3T^2 + 3r_3s_6}{s_5s_6T^4 + 4r_3s_5T^3 + 12r_3s_6T + 12r_3^2}x_6(t) \end{aligned} \quad (81)$$

The required acceleration along each axis can now be obtained by making the sum of the actual and gravity acceleration equal to the total required acceleration, thus

$$u^o(t) = a(t) + g(t) \quad (82)$$

or

$$a(t) = u^o(t) - g(t) \quad (83)$$

for each component. By using $u_1(t) - g_1(t)$; $u_2(t) - g_2(t)$ and $u_3(t) - g_3(t)$ it is possible to determine the optimal acceleration for each axis. Furthermore, constraining equations such as the constraining relationship between the length of a and the three components of a can readily be added. For example, if an engine is throttleable as well as gimbaled, such a constraint can be satisfied by ensuring that

$$|a_T| = (a_{T_x}^2 + a_{T_y}^2 + a_{T_z}^2)^{\frac{1}{2}} \quad (84)$$

where the direction cosines of the desired thrust direction given by

$$\cos \alpha = \frac{a_{T_x}}{a_T} \quad (85)$$

$$\cos \beta = \frac{a_{T_y}}{a_T} \quad (86)$$

$$\cos \gamma = \frac{a_{T_z}}{a_T} \quad (87)$$

The above commands have been calculated in the inertial frame and need to be transformed to the body frame, before they can be applied to the air-frame, as discussed in Section 3.5. For $r_1 = r_2 = r_3 = r$, $s_1 = s_3 = s_5 = s$, and $s_2 = s_4 = s_6 = s$ the general optimal navigation law can be written as

$$u_i^o(t) = - \frac{6sT(sT + 2r)}{s^2T^4 + 4rsT^3 + 12rsT + 12r^2} x_i(t) - \frac{4(s^2T^3 + 3sT^2 + 3rs)}{s^2T^4 + 4rsT^3 + 12rsT + 12r^2} x_{i+1}(t). \quad (88)$$

To demonstrate the linear-quadratic approach, an example is presented of a low order nonlinear system given by

$$\dot{x} = v \quad (89)$$

$$\dot{v} = a - \frac{1}{x^2} = u$$

with the performance criterion

$$J = \frac{1}{2} x^T S x + \frac{1}{2} \int_0^t u^2 dt \quad (90)$$

From the previous section, the optimal control for $r = 1$ is given by

$$u^o(t) = - \frac{6s_1T(s_2T + 2)}{s_1s_2T^4 + 4s_1T^3 + 12s_2T + 12}x_1(t) - \frac{4(s_1s_2T^3 + 3s_1T^2 + 3s_2)}{s_1s_2T^4 + 4s_1T^3 + 12s_2T + 12}x_2(t) \quad (91)$$

and for $s_1 = s_2 = 2$

$$u^o(t) = - \frac{6T(T + 1)}{T^4 + 2T^3 + 6T + 3}x_1(t) - \frac{4T^3 + 6T^2 + 6}{T^4 + 2T^3 + 6T + 3}x_2(t) \quad (92)$$

This optimal control u now has to satisfy the condition that $u^o = -\frac{1}{x^2} + a$, i.e. of the total control requirement u_o , part $-\frac{1}{x^2}$, is provided by the dynamics of the vehicle, while the remaining part $a = u + \frac{1}{x^2}$ needs to be provided by the guidance computer.

2.5 Midcourse Navigation Law Evaluation

The above optimal navigation law has been implemented on ATS's adjoint simulation (See Appendix A for a description of the simulation). A second order autopilot with damping ration of .7 and a natural frequency of 5 rad/sec and an airframe time constant of 2.5 sec, was used in the studies.

Miss distance sensitivity runs with changes in the location of the handover-to-terminal navigation point caused by updates in the point from the ground are shown in Figure 1.

The results show that with no update or with an update prior to 5 seconds-to-go the resulting miss distance is negligible. Worst case updates would occur if they were transmitted at .25, .5 or 1.5 seconds-to-go.

The midcourse navigation law development and the above miss-distance results assume that there are no errors in the inertial navigation system (INS) of the vehicle. In real life however, errors caused by initialization or instrument drifts of the INS will contribute to the miss distance at handover. Determination of those errors will require an error analysis of the INS, analysis of the transfer alignment from the master inertial reference system to the INS before launch, which may include the estimation and updating of the INS gyro drifts and accelerometer biases. However, should the results of such a study and the mission requirements indicate that a more accurate INS is required, it could be achieved by updating the vehicle's position from the ground and so correct for any INS errors that may have accrued during midcourse flight. The timing requirements for this INS update will follow a similar pattern as shown in Figure 1. Figure 2 shows the sensitivity of guidance error to update accuracy as a function of range.

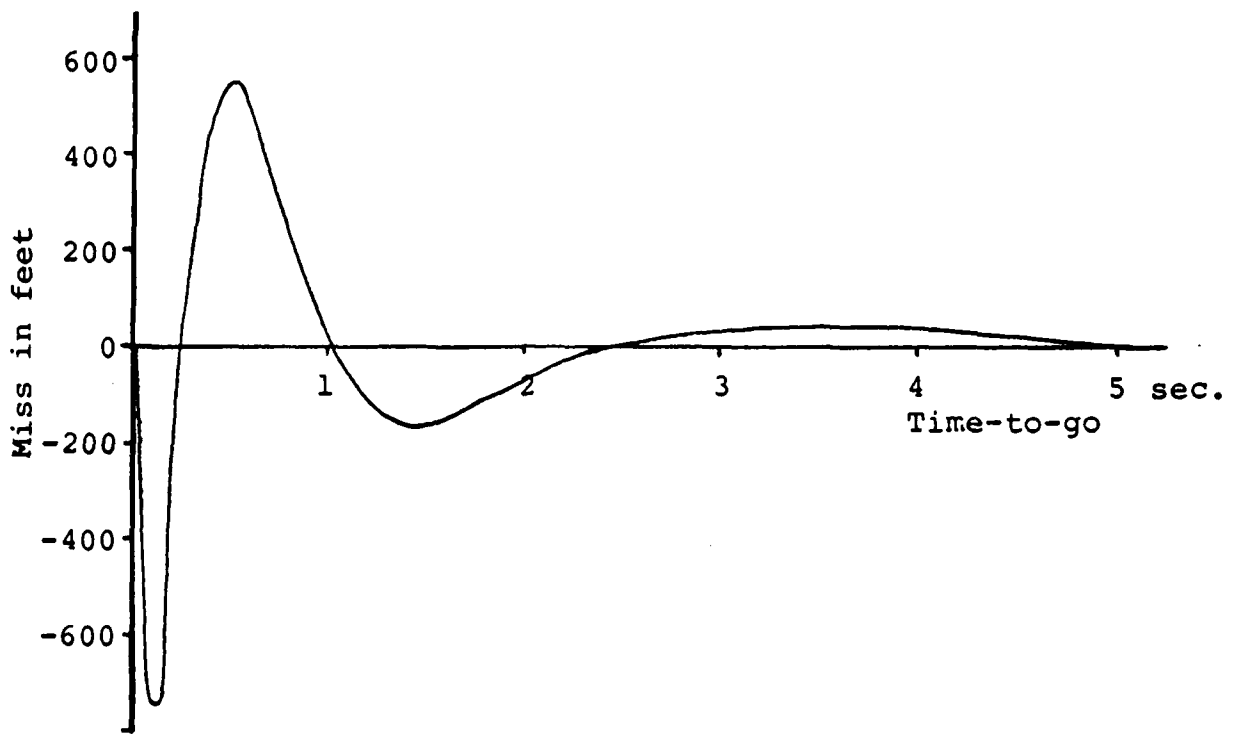


Fig. 1: Miss-Distance Sensitivity with a Step Displacement in Handover-to-Terminal Point versus Time-to-Go.

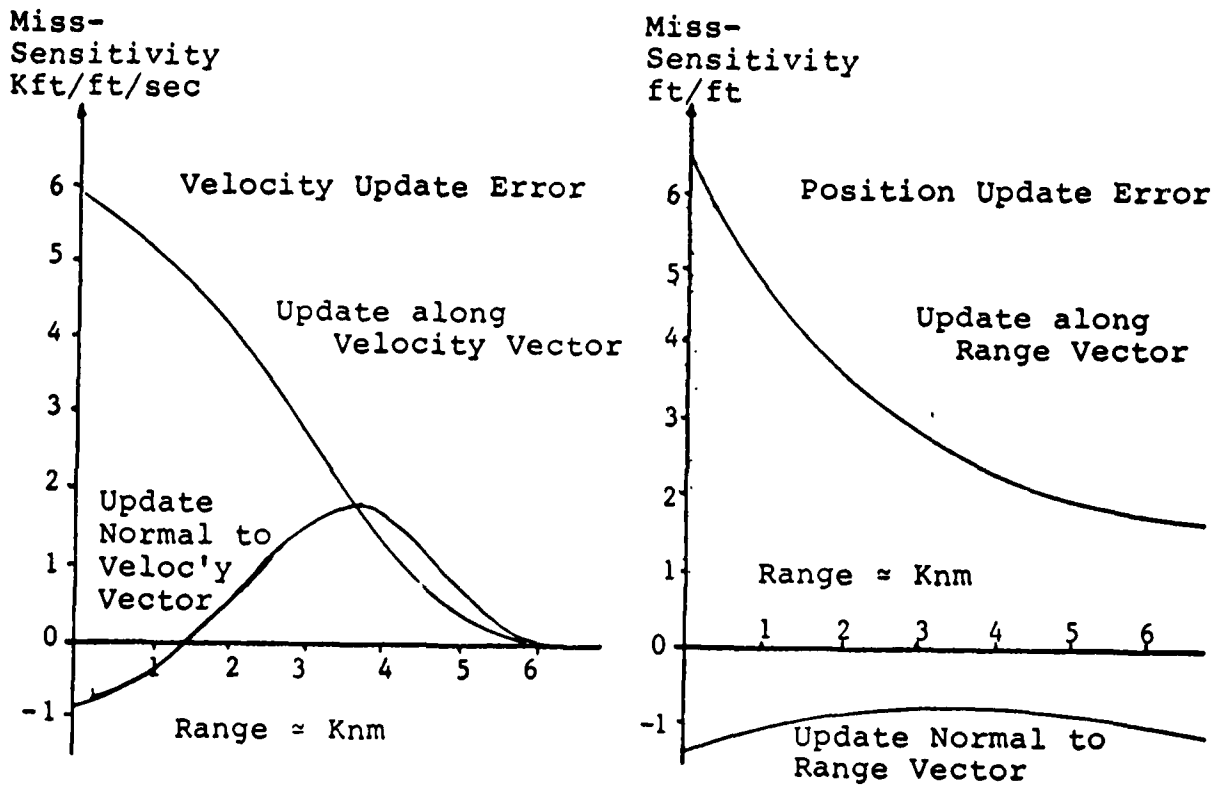


Fig. 2: Guidance Error Sensitivity to Update Accuracy

The midcourse guidance errors will result in a missile-to-target line-of-sight pointing error during the acquisition phase at handover and are reflected in the seeker field of view requirements.

If R is the missile-to-target range vector at launch and M and T the missile and target position vectors at handover to terminal guidance, then $RMT = R - M - T$ is the range vector from missile to target at handover. If at handover to terminal guidance the error in target position due to the target prediction error is $\Delta T = T\Delta\theta_T$ and if the error in missile location at that time is $\Delta M = M\Delta\theta_M$ then the maximum look angle error is

$$\Delta\beta = \frac{\Delta M + \Delta T}{RMT} = \frac{M\Delta\theta_M + T\Delta\theta_T}{V_c Tgo} \quad (93)$$

and if $\Delta\theta_M$ and $\Delta\theta_T$ are independent normal random variables, then

$$\sigma^2_{\Delta\beta} = \frac{M^2\sigma^2_{\theta M} + T^2\sigma^2_{\theta T}}{V_c^2 Tgo^2} \quad (94)$$

For a balanced system where $M\sigma_{\theta M} = T\sigma_{\theta T} = R_I\sigma_{\theta}$ the rms look-angle error is

$$\sigma_{\Delta\beta} = \frac{\sqrt{2}R_I\sigma_{\theta}}{V_c Tgo} \quad (95)$$

where

R_I is the range to intercept

V_c is the missile-target closing velocity

Tgo is the time-to-go

The probability that the radius of the field-of-view requirement r is less than a given value R is defined by

$$P(r < R) = 1 - e^{R^2/2\sigma^2_{\Delta\beta}} \quad (96)$$

or

$$R = -\sqrt{2}\sigma_{\Delta\beta}[-\ln(1 - P(r < R))]^{\frac{1}{2}} \quad (97)$$

Substituting $\sigma_{\Delta\beta}$ from Eqn (95) gives

$$R = \frac{2R_I}{V_c Tgo} \sigma_{\Delta\theta} [-\ln(1 - P(r < R))]^{\frac{1}{2}} \quad (98)$$

and the total field of view requirement is then

$$D = \frac{4R_I}{V_c Tgo} \sigma_{\Delta\theta} [-\ln(1 - P(r < R))]^{\frac{1}{2}} \quad (99)$$

For an R_I of 200,000 ft, a V_c of 10,000 ft/sec, and a $\sigma_{\Delta\theta}$ of 10 millirad the field of view requirements at various times-to-go and for probabilities of target containment of .9, .99 and .999 are shown in Table I.

Probability of Containment	Tgo sec	FOV degrees
.9	20	3.5
	10	7.0
	5	13.9
.99	20	4.9
	10	9.8
	5	19.7
.999	20	6.0
	10	12.5
	5	24.1

Table I: Seeker Field of View Requirements

3.0 OPTIMAL TERMINAL NAVIGATION LAW DEVELOPMENT

3.1 Introduction

Development of the terminal navigation law closely parallels the development of the midcourse navigation law. However, because of a possible moving target, the differential equations of the target have been included in the dynamic model equations, increasing the number of state variables from six to nine. In addition, since the final time is now a free parameter, it has to be estimated and methods to estimate time-to-go have to be developed. Furthermore, since terminal navigation information is obtained from a terminal sensor, the stochastic aspects of this sensor, as well as boresight error slope (discussed below) have to be included in the evaluation of the resulting navigation law.

3.2 Terminal Navigation Law Formulation

Similar to the midcourse navigation law, the two-point boundary value problem for the terminal navigation law consists of the vehicle's current position and velocity vectors

$$r(t_o) = (x_o, y_o, z_o) \quad (100)$$

$$v(t_o) = (\dot{x}_o, \dot{y}_o, \dot{z}_o) \quad (101)$$

and the required position and velocity vectors at intercept

$$r(t_f) = (x_f, y_f, z_f) \quad (102)$$

$$v(t_f) = (\dot{x}_f, \dot{y}_f, \dot{z}_f) \quad (103)$$

The requirement is to find the acceleration vector program for $t_o \leq t \leq t_f$ that drives the vehicle from its present position to intercept. As before, the total required acceleration profile will be obtained and the nonlinear gravity terms are then taken into account in a way that necessitates no approximations.

If we define the state vector with

x_1 = the target/vehicle relative position in the x direction

x_2 = the target/vehicle relative position in the y direction

x_3 = the target/vehicle relative position in the z direction

x_4 = the target/vehicle relative velocity in the x direction

x_5 = the target/vehicle relative velocity in the y direction

x_6 = the target/vehicle relative velocity in the z direction

x_7 = the target/vehicle relative acceleration in the x direction

x_8 = the target/vehicle relative acceleration in the y direction

x_9 = the target/vehicle relative acceleration in the z direction

and if we further assume that the target acceleration can be modeled as a first order process, i.e. $\dot{a}_T = -\tau a_T$ then we can formulate a set of first order linear differential

equations which describe the system dynamics in state variable form, i.e.

$$\begin{aligned}
 \dot{x}_1 &= x_4 \\
 \dot{x}_2 &= x_5 \\
 \dot{x}_3 &= x_6 \\
 \dot{x}_4 &= x_7 - a_x \\
 \dot{x}_5 &= x_8 - a_y \\
 \dot{x}_6 &= x_9 - a_z \\
 \dot{x}_7 &= -\tau_1 x_7 \\
 \dot{x}_8 &= -\tau_2 x_8 \\
 \dot{x}_9 &= -\tau_3 x_9
 \end{aligned} \tag{104}$$

If the control vector, u , is defined to be the missile acceleration, then the state model can be written such that

$$\dot{x} = Ax + Bu \tag{105}$$

where

$$A = \begin{pmatrix} 0_3 & I_3 & 0_3 \\ 0_3 & 0_3 & I_3 \\ 0_3 & 0_3 & -\tau_i I_3 \end{pmatrix} \quad B = \begin{pmatrix} 0_3 \\ -I_3 \\ 0_3 \end{pmatrix} \tag{106}$$

and

$$x = \begin{pmatrix} x_1 \\ x_2 \\ x_3 \\ x_4 \\ x_5 \\ x_6 \\ x_7 \\ x_8 \\ x_9 \end{pmatrix} \quad u = \begin{pmatrix} a_x \\ a_y \\ a_z \end{pmatrix} \tag{107}$$

3.3 Optimal Control Formulation

The performance criterion to be minimized is given by

$$J = \frac{1}{2} x^T(t_f) S_f x(t_f) + \frac{1}{2} \int_{t_0}^{t_f} (u^T R u) dt \tag{108}$$

where

$$S = \begin{pmatrix} s_3 & 0 & 0 \\ 0 & 0 & 0 \\ 0 & 0 & 0 \end{pmatrix} \text{ with } S_3 = \begin{pmatrix} s_1 & 0 & 0 \\ 0 & s_2 & 0 \\ 0 & 0 & s_3 \end{pmatrix} \text{ and } R = \begin{pmatrix} r_1 & 0 & 0 \\ 0 & r_2 & 0 \\ 0 & 0 & r_3 \end{pmatrix} \tag{109}$$

This cost functional has no weighting on the final relative velocity nor on the target acceleration, but has a weighted cost on the control or vehicle acceleration through the integral term. In this Phase I Study, each of the weighting parameters will be treated as a generic variable and will thus appear explicitly in the solution.

3.4 Optimal Control Solution

Using Eqns (105) and (108) the Hamiltonian is constructed as follows

$$H = \frac{1}{2}u^T R u + \lambda^T (Ax + Bu) \quad (110)$$

where λ is now a co-state vector with dimension 9×1 . The necessary conditions for optimality are then

$$\dot{\lambda} = -H_x = -A^T \lambda \quad (111)$$

$$0 = H_u = Ru + B^T \lambda \quad (112)$$

This last equation can be re-written as

$$u^o = -R^{-1}B^T \lambda \quad (113)$$

Substituting Eqn (113) into Eqn (105) provides

$$\dot{x} = Ax - BR^{-1}B^T \lambda \quad (114)$$

Thus we can write Eqns (111) and (114)

$$\begin{pmatrix} \dot{x} \\ \dot{\lambda} \end{pmatrix} = \begin{pmatrix} A & -BR^{-1}B^T \\ 0 & -A^T \end{pmatrix} \begin{pmatrix} x \\ \lambda \end{pmatrix} \quad (115)$$

with boundary conditions $x(t_o)$ and $\lambda(t_f) = S_f x(t_f)$. Writing out the $\dot{\lambda}$ part of Eqn (115) we have

$$\begin{aligned} \dot{\lambda}_1 &= 0 \\ \dot{\lambda}_2 &= 0 \\ \dot{\lambda}_3 &= 0 \\ \dot{\lambda}_4 &= -\lambda_1 \\ \dot{\lambda}_5 &= -\lambda_2 \\ \dot{\lambda}_6 &= -\lambda_3 \\ \dot{\lambda}_7 &= \tau_1 \lambda_7 - \lambda_4 \\ \dot{\lambda}_8 &= \tau_2 \lambda_8 - \lambda_5 \\ \dot{\lambda}_9 &= \tau_3 \lambda_9 - \lambda_6 \end{aligned} \quad (116)$$

Integrating this equation from t_f to t gives

$$\begin{aligned}
 \lambda_1(t) &= s_1 x_1(t_f) \\
 \lambda_2(t) &= s_2 x_2(t_f) \\
 \lambda_3(t) &= s_3 x_3(t_f) \\
 \lambda_4(t) &= -s_1 x_1(t_f)(t - t_f) \\
 \lambda_5(t) &= -s_2 x_2(t_f)(t - t_f) \\
 \lambda_6(t) &= -s_3 x_3(t_f)(t - t_f)
 \end{aligned} \tag{117}$$

and the resulting optimal control is from equation (79)

$$u^o(t) = \begin{pmatrix} \frac{s_1}{r_1} T & 0 & 0 \\ 0 & \frac{s_2}{r_2} T & 0 \\ 0 & 0 & \frac{s_3}{r_3} T \end{pmatrix} x(t_f) \tag{118}$$

The \dot{x} part of Eqn (115) can now be written out as

$$\begin{aligned}
 \dot{x}_1 &= x_4 \\
 \dot{x}_2 &= x_5 \\
 \dot{x}_3 &= x_6 \\
 \dot{x}_4 &= x_7 - \frac{1}{r_1} \lambda_4 = x_7 - \frac{s_1}{r_1} x_1(t_f) T \\
 \dot{x}_5 &= x_8 - \frac{1}{r_2} \lambda_5 = x_8 - \frac{s_2}{r_2} x_2(t_f) T \\
 \dot{x}_6 &= x_9 - \frac{1}{r_3} \lambda_6 = x_9 - \frac{s_3}{r_3} x_3(t_f) T \\
 \dot{x}_7 &= -r_1 x_7 \\
 \dot{x}_8 &= -r_2 x_8 \\
 \dot{x}_9 &= -r_3 x_9
 \end{aligned} \tag{119}$$

with boundary conditions at $t_o = x(0)$ and $T = t_f - t$. Integrating the bottom three equations from t_o to t gives

$$\begin{aligned}
 x_7(t) &= e^{-r_1(t-t_o)} x_7(t_o) \\
 x_8(t) &= e^{-r_2(t-t_o)} x_8(t_o) \\
 x_9(t) &= e^{-r_3(t-t_o)} x_9(t_o)
 \end{aligned} \tag{120}$$

The next set of differential equations can then be written as

$$\begin{aligned}
 \dot{x}_4(t) &= e^{-r_1(t-t_o)} x_7(t_o) + \frac{s_1}{r_1} x_1(t_f)(t - t_o) - \frac{s_1}{r_1} x_1(t_f)(t_f - t_o) \\
 \dot{x}_5(t) &= e^{-r_2(t-t_o)} x_8(t_o) + \frac{s_2}{r_2} x_2(t_f)(t - t_o) - \frac{s_2}{r_2} x_2(t_f)(t_f - t_o) \\
 \dot{x}_6(t) &= e^{-r_3(t-t_o)} x_9(t_o) + \frac{s_3}{r_3} x_3(t_f)(t - t_o) - \frac{s_3}{r_3} x_3(t_f)(t_f - t_o)
 \end{aligned} \tag{121}$$

Integrating Eqn (121) from t_o to t gives

$$\begin{aligned}x_4(t) &= \frac{1}{r_1}(1 - e^{-r_1(t-t_o)})x_7(t_o) + \frac{s_1}{r_1}x_1(t_f)(t - t_o)^2 - \frac{s_1}{r_1}x_1(t_f)(t_f - t_o)(t - t_o) + x_4(t_o) \\x_5(t) &= \frac{1}{r_2}(1 - e^{-r_2(t-t_o)})x_8(t_o) + \frac{s_2}{r_2}x_2(t_f)(t - t_o)^2 - \frac{s_2}{r_2}x_2(t_f)(t_f - t_o)(t - t_o) + x_5(t_o) \\x_6(t) &= \frac{1}{r_3}(1 - e^{-r_3(t-t_o)})x_9(t_o) + \frac{s_3}{r_3}x_3(t_f)(t - t_o)^2 - \frac{s_3}{r_3}x_3(t_f)(t_f - t_o)(t - t_o) + x_6(t_o)\end{aligned}\quad (122)$$

The results for $x_1(t)$, $x_2(t)$ and $x_3(t)$ can then be obtained by integrating the above three equations from t_o to t resulting in

$$\begin{aligned}x_1(t) &= \frac{t - t_o}{r_1}x_7(t_o) - \frac{1}{r_1^2}(1 - e^{-r_1(t-t_o)})x_7(t_o) + \frac{s_1}{6r_1}x_1(t_f)(t - t_o)^3 - \\&\quad \frac{s_1}{2r_1}x_1(t_f)(t_f - t_o)(t - t_o)^2 + x_4(t_o)(t - t_o) + x_1(t_o) \\x_2(t) &= \frac{t - t_o}{r_2}x_8(t_o) - \frac{1}{r_2^2}(1 - e^{-r_2(t-t_o)})x_8(t_o) + \frac{s_2}{6r_2}x_2(t_f)(t - t_o)^3 - \\&\quad \frac{s_2}{2r_2}x_2(t_f)(t_f - t_o)(t - t_o)^2 + x_5(t_o)(t - t_o) + x_2(t_o) \\x_3(t) &= \frac{t - t_o}{r_3}x_9(t_o) - \frac{1}{r_3^2}(1 - e^{-r_3(t-t_o)})x_9(t_o) + \frac{s_3}{6r_3}x_3(t_f)(t - t_o)^3 - \\&\quad \frac{s_3}{2r_3}x_3(t_f)(t_f - t_o)(t - t_o)^2 + x_6(t_o)(t - t_o) + x_3(t_o)\end{aligned}\quad (123)$$

The above results can be put into shorthand notation for $t = t_f$, and $T = t_f - t_o$, resulting in

$$\begin{aligned}\left(\frac{s_1}{r_1}T^3 + 1\right)x_1(t_f) &= x_1(t_o) + Tx_4(t_o) - \frac{1}{r_1^2}(1 - e_1)x_7(t_o) \\ \left(\frac{s_2}{r_2}T^3 + 1\right)x_2(t_f) &= x_2(t_o) + Tx_5(t_o) - \frac{1}{r_2^2}(1 - e_2)x_8(t_o) \\ \left(\frac{s_3}{r_3}T^3 + 1\right)x_3(t_f) &= x_3(t_o) + Tx_6(t_o) - \frac{1}{r_3^2}(1 - e_3)x_9(t_o) \\ \frac{s_1}{2r_1}T^2x_1(t_f) + x_4(t_f) &= x_4(t_o) + \frac{1}{r_1}(1 - e_1)x_7(t_o) \\ \frac{s_2}{2r_2}T^2x_2(t_f) + x_5(t_f) &= x_5(t_o) + \frac{1}{r_2}(1 - e_2)x_8(t_o) \\ \frac{s_3}{2r_3}T^2x_3(t_f) + x_6(t_f) &= x_6(t_o) + \frac{1}{r_3}(1 - e_3)x_9(t_o) \\ x_7(t_f) &= e^{-r_1T}x_7(t_o) = e_1x_7(t_o) \\ x_8(t_f) &= e^{-r_2T}x_8(t_o) = e_2x_8(t_o) \\ x_9(t_f) &= e^{-r_3T}x_9(t_o) = e_3x_9(t_o)\end{aligned}\quad (124)$$

and in matrix notation

$$\begin{bmatrix} \frac{s_1}{r_1}T^3 + 1 & 0 & 0 & 0 & 0 & 0 & 0 & 0 & 0 \\ 0 & \frac{s_2}{r_2}T^3 + 1 & 0 & 0 & 0 & 0 & 0 & 0 & 0 \\ 0 & 0 & \frac{s_3}{r_3}T^3 + 1 & 0 & 0 & 0 & 0 & 0 & 0 \\ \frac{s_1}{2r_1}T^2 & 0 & 0 & 1 & 0 & 0 & 0 & 0 & 0 \\ 0 & \frac{s_2}{2r_2}T^2 & 0 & 0 & 1 & 0 & 0 & 0 & 0 \\ 0 & 0 & \frac{s_3}{2r_3}T^2 & 0 & 0 & 1 & 0 & 0 & 0 \\ 0 & 0 & 0 & 0 & 0 & 0 & 1 & 0 & 0 \\ 0 & 0 & 0 & 0 & 0 & 0 & 0 & 1 & 0 \\ 0 & 0 & 0 & 0 & 0 & 0 & 0 & 0 & 1 \end{bmatrix} \quad (125)$$

$$x(t_f) = \begin{bmatrix} 1 & 0 & 0 & T & 0 & 0 & -\frac{E_1}{r_1} & 0 & 0 \\ 0 & 1 & 0 & 0 & T & 0 & 0 & -\frac{E_2}{r_2} & 0 \\ 0 & 0 & 1 & 0 & 0 & T & 0 & 0 & -\frac{E_3}{r_3} \\ 0 & 0 & 0 & 1 & 0 & 0 & E_1 & 0 & 0 \\ 0 & 0 & 0 & 0 & 1 & 0 & 0 & E_2 & 0 \\ 0 & 0 & 0 & 0 & 0 & 1 & 0 & 0 & E_3 \\ 0 & 0 & 0 & 0 & 0 & 0 & e_1 & 0 & 0 \\ 0 & 0 & 0 & 0 & 0 & 0 & 0 & e_2 & 0 \\ 0 & 0 & 0 & 0 & 0 & 0 & 0 & 0 & e_3 \end{bmatrix} x(t_o) \quad (126)$$

where $e_i = e^{-r_i T}$ and $E_i = \frac{1}{r_i}(1 - e_i)$. By rewriting the coefficient matrix as

$$\begin{bmatrix} 11 & 0 & 0 & 0 & 0 & 0 & 0 & 0 & 0 \\ 0 & 22 & 0 & 0 & 0 & 0 & 0 & 0 & 0 \\ 0 & 0 & 33 & 0 & 0 & 0 & 0 & 0 & 0 \\ 41 & 0 & 0 & 1 & 0 & 0 & 0 & 0 & 0 \\ 0 & 52 & 0 & 0 & 1 & 0 & 0 & 0 & 0 \\ 0 & 0 & 63 & 0 & 0 & 1 & 0 & 0 & 0 \\ 0 & 0 & 0 & 0 & 0 & 0 & 1 & 0 & 0 \\ 0 & 0 & 0 & 0 & 0 & 0 & 0 & 1 & 0 \\ 0 & 0 & 0 & 0 & 0 & 0 & 0 & 0 & 1 \end{bmatrix} \quad (127)$$

its inverse has been obtained, resulting in

$$\begin{bmatrix} \frac{1}{11} & 0 & 0 & 0 & 0 & 0 & 0 & 0 & 0 \\ 0 & \frac{1}{22} & 0 & 0 & 0 & 0 & 0 & 0 & 0 \\ 0 & 0 & \frac{1}{33} & 0 & 0 & 0 & 0 & 0 & 0 \\ -\frac{41}{11} & 0 & 0 & 1 & 0 & 0 & 0 & 0 & 0 \\ 0 & -\frac{52}{22} & 0 & 0 & 1 & 0 & 0 & 0 & 0 \\ 0 & 0 & -\frac{63}{33} & 0 & 0 & 1 & 0 & 0 & 0 \\ 0 & 0 & 0 & 0 & 0 & 0 & 1 & 0 & 0 \\ 0 & 0 & 0 & 0 & 0 & 0 & 0 & 1 & 0 \\ 0 & 0 & 0 & 0 & 0 & 0 & 0 & 0 & 1 \end{bmatrix} \quad (128)$$

Post-multiplying Eqn (118) with Eqn (128) and the right-hand side of Eqn (125) which is Eqn (126), substituting the actual terms from the coefficient matrix and letting the current time $4t = t_o$, results in the continuous optimal feedback navigation law with

$$\begin{aligned} u_1^o(t) &= -\frac{3s_1T}{s_1T^3 + 3r_1}x_1(t) - \frac{3s_1T^2}{s_1T^3 + 3r_1}x_4(t) + \frac{3s_1(1-e_1)T}{\tau_1^2(s_1T^3 + 3r_1)}x_7(t) \\ u_2^o(t) &= -\frac{3s_2T}{s_2T^3 + 3r_2}x_2(t) - \frac{3s_2T^2}{s_2T^3 + 3r_2}x_5(t) + \frac{3s_2(1-e_2)T}{\tau_2^2(s_2T^3 + 3r_2)}x_8(t) \\ u_3^o(t) &= -\frac{3s_3T}{s_3T^3 + 3r_3}x_3(t) - \frac{3s_3T^2}{s_3T^3 + 3r_3}x_6(t) + \frac{3s_3(1-e_3)T}{\tau_3^2(s_3T^3 + 3r_3)}x_9(t) \end{aligned} \quad (129)$$

If we let $r = r = 0$ and $s = 1$ in the above guidance laws, then $u = -3[\frac{z_i}{T^2} + \frac{\dot{z}_i}{T}]$. If we now let V = closing velocity along the line-of-sight and $\sigma = x_i/T$ = the line-of-sight angle, then $u_i = -3V\dot{\sigma}$, which is the well known proportional navigation law with a navigation ratio of 3.

3.5 Estimating Time-to-go and Target Acceleration

The necessity of knowledge of time-to-go (Tgo) arises from the fact that during the development of the guidance law the final time was assumed fixed while it also assumed complete control of all three vehicle acceleration components. In real life, both those assumptions will have to be evaluated for application of navigation laws to various vehicles. When the rocket engine thrust magnitude is fixed, the solution of Tgo is unique. When the rocket engine is throttleable there is a certain latitude in the choice of Tgo for there is then additional flexibility in the allocation of thrust acceleration. A Tgo algorithm can then be developed, assuming zero target acceleration, and then be expanded to include target acceleration. Furthermore, some information such as target acceleration for terminal navigation implementation is not directly available and requires the development of an on-board extended Kalman Filter.

An important issue which needs to be addressed concerns the interfacing of the navigation and estimation algorithms with the terminal sensors, the airframe sensors, and the

autopilot. The terminal sensor measurement with the sensor gimbal angles provide information referenced to body coordinates and are corrupted by noise. The autopilot uses the navigation commands after transformation from the inertial- to the body fixed frame to maneuver the airframe, which is sensed by on-board dynamic sensors and is fed back to the autopilot, to provide system stability. This motion is also sensed by the terminal sensor thus closing the kinematic loop. The dynamic sensors for a similar set are also used to update the on-board inertial reference frame used for the navigation equation. Thus the coordinate frame transformation between the terminal-sensor, the body frame, and the inertial frame need to be considered.

One of the most important considerations in the design of homing missile systems is the effect of body motion coupling onto the signal. Body motion coupling arises mainly from the distortion of the incoming target return energy as it passes the radome which protects the sensor and antenna assembly in the nose of the missile. This issue is further addressed in the next section.

3.6 Radome Boresight Errors

One of the main concerns that must be addressed when designing sensor hardware and guidance laws for homing missiles is that of radome/optical window boresight error interactions. Boresight errors arise from the distortion of the incoming energy wavefront as it passes through the missile's radome/optical window.

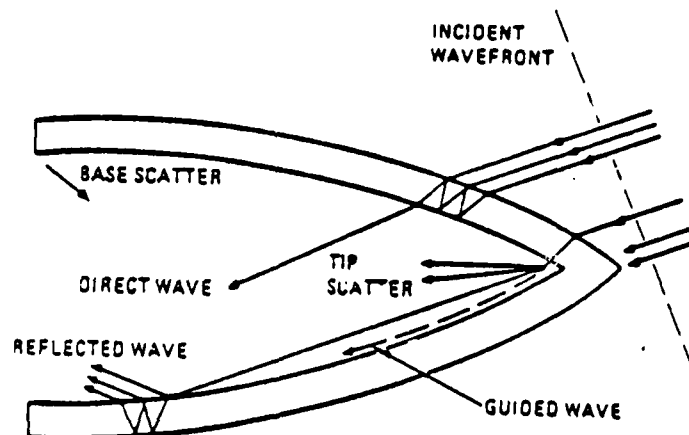


Fig. 3: Wave Mechanism in Hollow Dielectric Shell

The principal contributor to this distortion is the non-symmetrical refraction of the wavefront that results when the energy confronts the different dielectric properties at the interface between the atmosphere and the non-hemispherically shaped radome. Typical wave mechanisms in a hollow dielectric shell are shown in Figure 3. Other contributors to wavefront distortion are internal reflections within the radome, channeling of energy

along the radome surface, and multipath and shadowing caused by other hardware near the nose of the missile.

The ultimate consequence of this wavefront distortion is an apparent tracking error induced by the radome/optical window. Hence the missile/target line-of-sight direction which is measured by the missile seeker appears to be perturbed from its true value. This perturbation is a strong function of the direction with respect to the radome from which the energy is coming, and thus is a function of the seeker look angle which in turn is a function of the pursuit geometry as it evolves over time. This dependence on the geometry creates body motion coupling that can alter the overall response of the missile system and modify the measured noise characteristics as discussed below.

The sensor/missile/target angular relationships are shown in Figure 4, and a simplified single-plane representation of a skid-to-turn homing missile guidance system is shown in Figure 5. Included in this latter figure is the body motion coupling feedback path caused by radome/optical window boresight interactions. This feedback path arises in the missile as follows. The missile/target line-of-sight vector σ is tracked by the missile's seeker and the output of the associated electronics forms an estimate of the rotation rate, $\dot{\sigma}$, of the line-of-sight vector. This measured line-of-sight rotation rate provides the principal guidance information for the homing missile.

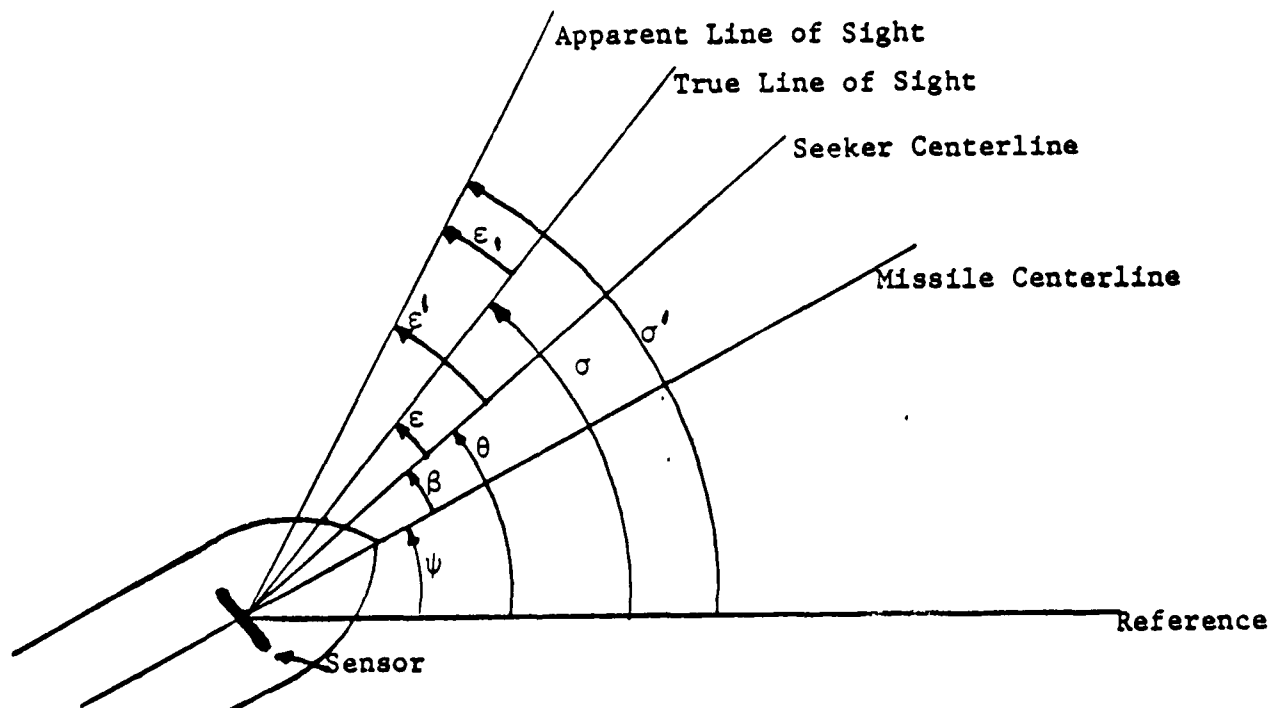


Fig. 4: Sensor/Missile/Target Angular Relationships

However, because of the radome boresight error the measured line-of-sight vector is

perturbed from its true direction σ by an angle ϵ_1 . Thus the apparent line-of-sight angle, σ' , can be written in terms of the true line-of-sight angle, σ , and the radome induced error as $\sigma' = \sigma + \epsilon_1$ and the apparent line-of-sight rate, $\dot{\sigma}'$, is then:

$$\frac{d\sigma'}{dt} = \frac{d\sigma}{dt} + \frac{\partial \epsilon_1}{\partial (\beta + \epsilon)} \frac{d(\beta + \epsilon)}{dt} \quad (130)$$

or

$$\dot{\sigma}' = \dot{\sigma} + r(\dot{\beta} + \dot{\epsilon}) \quad (131)$$

where r is known as the boresight error slope, i.e. the change of boresight error for a change in seeker gimbal look angle.

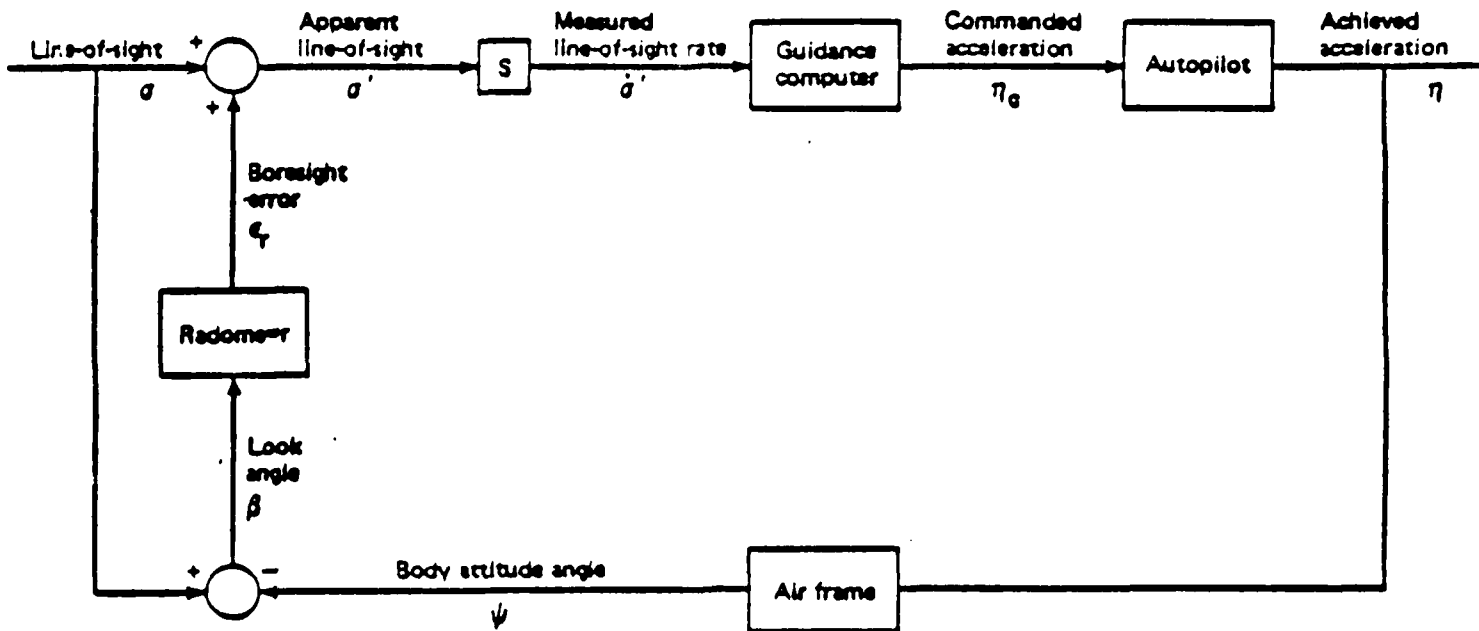


Fig. 5: Missile Guidance System. Showing Boresight Error Feedback

But $\dot{\beta} = \dot{\epsilon} = \dot{\sigma} - \dot{\psi}$, where $\dot{\sigma}$ is the look angular rate, and $\dot{\psi}$ is the missile body rotation rate. Hence the measured line-of-sight rate can thus be expressed as

$$\dot{\sigma}' = (1 + r)\dot{\sigma} + r\dot{\psi} \quad (132)$$

This equation illustrates the major effects of radome/optical window boresight errors on the measured guidance signal. First the radome error modifies the gain from the true guidance signal, $\dot{\sigma}$, to the measured guidance signal, $\dot{\sigma}'$. Second, and by far the most important effect is that it couples body motion, $\dot{\psi}$, onto the measured guidance

signal, $\delta\theta$. The presence of this term results in the closing of an outer feedback path around the airframe, identical to the standard rate gyro feedback path used in autopilot design to achieve airframe stability, and thus can alter the system response and stability characteristics. In particular, as the value of r becomes more negative, the effective missile system time constant decreases. On the other hand, as r becomes more positive, the missile system time constant increases, resulting in a more sluggish system response.

There are a number of loop parameters which affect the sensitivity of the system to the positive and negative values of the boresight error slopes. In the guidance computer, both the guidance gain and the guidance time constant affect the neutral stability slopes. If the guidance gain is decreased, the body motion coupling gain also decreases, and a larger value of $|r|$ can be tolerated. Increasing the guidance filter time constant decreases the loop gain at high frequencies. Hence, increasing the guidance filter time constant increases the neutrally stable boresight error slope.

A parameter which typically can not be modified during guidance system design, but which also greatly affects missile behavior is the effective airframe lift coefficient A (in g's per degree of angle-of-attack). In general, as the magnitude of the effective lift coefficient, A , decreases, the body motion feedback loop gain associated with the airframe block in Figure 5 increases. Consequently, for low lift airframes the effect of the radome boresight errors on missile performance characteristics becomes more pronounced.

When a radome induced instability occurs in a missile an oscillation begins to develop in the missile's steering control channels. This can lead to a number of phenomena which degrade missile performance:

1. When the boresight error slope is negative the instability exists at a low frequency well within the guidance bandwidth of the system. The missile's response to the undesirable steering command is thus unattenuated and the missile may deviate radically from its desired trajectory, resulting in large miss distances.
2. If an instability occurs due to a large positive boresight error slope, it results in an oscillation which is of high enough frequency that it is typically attenuated by the missile airframe dynamics. Trajectory anomalies are now caused by dynamic range constraints within the guidance/autopilot system and manifest themselves principally as clipping or limiting of the oscillatory guidance signal. The clipping results in an effective reduction in the guidance gain from its design value, thus impairing system performance.

An important property of the radome induced instability is that the resulting oscillation does not necessarily continue to grow in amplitude. Figure 6 illustrates a typical two-dimensional boresight error characteristic as a function of the geometric look angle, β . Suppose that nominally the missile/target line-of-sight vector is offset from the missile

centerline by a look angle of β_0 , and that the magnitude of the boresight error slope r at β_0 is larger than the critically stable slope r_c . As a result, the system will begin to go unstable. The missile steering oscillation starts to grow and the missile centerline begins to rotate relative to the inertially fixed missile/target line-of-sight vector. As the look angle oscillation increases in amplitude, averaging of the boresight error occurs. In fact, the oscillation will increase only until the average boresight error slope equals r_c . If the oscillation were to increase further, the average slope would be less than the critical slope, implying stability, and consequently the oscillation would die down until the average slope was again at least r_c .

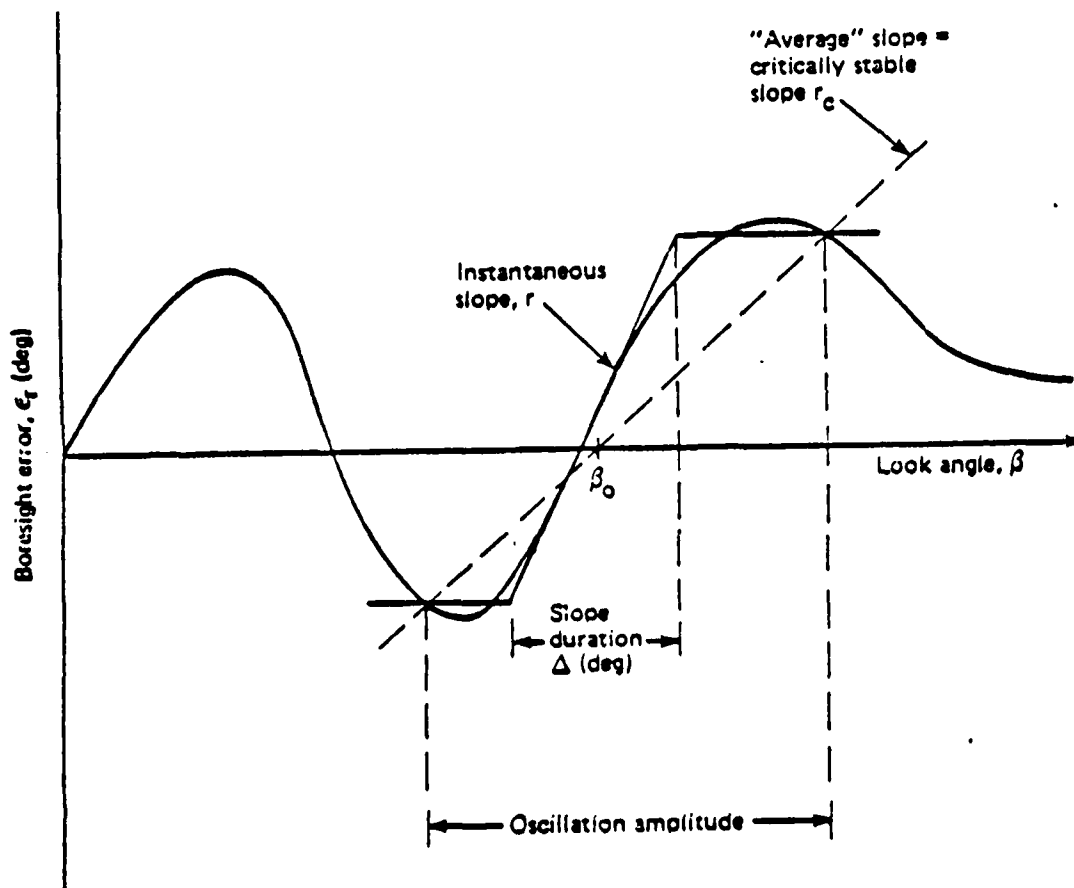


Fig. 6: Illustration of Relationship between Boresight Error Characteristics and Oscillation Amplitude

It is through this mechanism that a bounded oscillation results. If the slope changes are fast enough the guidance system characteristics will be determined by an effective

slope rather than the instantaneous slope and the two can be substantially different. The three parameters that need to be considered are thus the critical boresight error slope r_c , the local or instantaneous slope r , and that local slope's duration in look angle Δ . In general, slopes that cover only a small region of the radome (i.e. small Δ) can be tolerated with much larger magnitudes than can slopes that persist over a large region of the radome.

The presence of radome induced instability does not automatically cancel the effectiveness of a missile. Rather, if boresight error characteristics are such that instability results in bounded oscillations of only small amplitudes, performance may still be quite satisfactory. Low frequency (negative r induced) trajectory deviations may be small and high frequency (positive r induced) guidance signal limiting may not be severe. ATS has taken advantage of this fact and developed, using dual-input describing function techniques, a method of boresight error compensation based on measured amplitudes and frequencies.

3.7 Terminal Navigation Law Evaluation

Determination of the terminal navigation law in terms of miss-distance would seem to require, in general, the complete solution of the trajectory equation subject to the appropriate driving and initial conditions. For practical control systems, however, it has been found impossible to obtain such solutions analytically. The difficulty arises from the fact that even a linearized trajectory equation:

1. has time-varying coefficients,
2. may be of quite a high order, the order being one higher than the number of time lags in the control system.

Thus one has to resort to simulation techniques to obtain miss-distance performance results. Even then, because of the time-varying coefficients, the cause-effect relationship is a function of two variables (one being the time of application, τ , of the cause and the other being the time of observation, t of the effect) and a straight forward simulation has to be run many times, each for a different maneuver application time, τ , which is a very costly and time-consuming process. American Technical Services (ATS) has overcome the computational difficulty with the use of an adjoint miss-distance simulation. The state transition matrix of an adjoint system is related to the state transition matrix of the original system by an interchange of the running time, t , and application time, τ , and a transposition. Thus, while the behavior of the system with respect to t is a function of the dynamics of the original system, the behavior of the system with respect to τ is a function of the dynamics of the adjoint system. As a result, the adjoint simulation requires only a single run to produce terminal miss-distance results due to each of the

initial conditions and each of the forcing functions and system disturbances. The adjoint technique of analysis is further discussed in Appendix A. In that appendix, Figure A-1 shows a block diagram of ATS's forward simulation with initial turning rate, heading and pointing errors, as well as target maneuver inputs and noise disturbances. Figure A-2 shows the block diagram of the corresponding adjoint simulation with outputs in terms of miss-distance due to initial turning rate, heading and pointing errors, as well as miss-distances due to each of the maneuvers and noise disturbances.

The terminal navigation law evaluation was performed using the adjoint simulation. The adjoint method of analysis is especially valuable when the system is subject to multiple input disturbances, since, as discussed in Appendix A, the sensitivities of the system output (i.e. terminal miss-distance) to the specific input disturbances are obtained with a single run at the outputs of the adjoint system.

Noise, and target glint noise in particular, has long been one of the primary concerns in assessing guidance performance. Noise interactions with radome boresight errors have not received much attention, since with a forward simulation it requires many runs, often hundreds, to obtain statistically meaningful results. The semi-active receiver noise model used in the adjoint simulation was based on the rms angular noise equation

$$\sigma_{\theta} = \frac{\theta_B}{k_m \sqrt{2S/N}} \quad (133)$$

and on the fact that the noise power density ($\theta(o)$) times the bandwidth equals the angular error squared ($\sigma_{\theta}^2 = \theta(o) * B\omega$), then

$$\theta(o) = \frac{\theta_B^2}{2k_m^2 S/N B\omega} \quad (134)$$

The form of the radar equation used for computation of the signal noise ratio is

$$S/N = \frac{P_a G_T G_w \lambda^2 \sigma_T}{(4\pi)^3 k T N_T L R_{IT}^2 R_{MT}^2 B\omega} \quad (135)$$

and thus

$$\theta(o) = \frac{(4\pi)^3 \theta_B^2 k T N_T L R_{IT}^2 R_{MT}^2}{2k_m^2 P_a G_T G_w \lambda^2 \sigma_T} \text{ rad}^2 / \text{Hz} / \text{ft}^2. \quad (136)$$

The range independent noise model used in the adjoint simulation used a noise power density of

$$\theta(o) = \frac{2}{12} \left(\frac{R}{2^N - 1} \right)^2 \Delta T \text{ rad}^2 / \text{Hz} \quad (137)$$

The glint noise model used is based on a model for a target that consists of scatterers distributed uniformly over the target length and is given by

$$\sigma_{gl} = 0.35L \text{ feet} \quad (138)$$

Target maneuver models consist of a target step displacement, a target step velocity and a target step acceleration, a filtered step acceleration, and a sinusoidal target acceleration. The initial condition errors consist of initial heading error turning rate, initial missile turning rate, and seeker pointing error. The miss distance results for zero boresight error slope due to target maneuver, initial heading error and initial turning rate are shown in Figure 7.

A boresight error model based on Eqn (132) was then implemented in the adjoint simulation and the miss distance sensitivity boresight error slopes determined. They were obtained by keeping the noise inputs constant and increasing the boresight error slopes for an rms miss distance due to glint noise twice the original value. The miss distance sensitivities of the glint, amplitude and receiver noise are shown in Figure 8.

The parameter values used in Eqns (134-139) for the missile are $\theta_B = .72$ deg, $kT = 4 \times 10^{-21}$ w/Hz, $N_f = 12$ db, $L = 15$ db, $k_m = 1.25$, $P_A = 3$ kW (100 kW peak), $G_T = 75$ db, $G_W = 49$ db, $\lambda = .0015$ m, $N = 15$ bits, $R = 50$ degrees and $\Delta = \frac{1}{30}$.

The rms miss distance result due to the semi-active receiver noise for a missile-target closing velocity of 10 kft/sec, a time constant of .1 sec and an illuminator-target range of 400 mi, is shown to be at .45 feet. The rms distance results due to the range independent noise is .48 feet.

For the major length (32.8 ft) of the target, the resulting rms miss distance due to glint noise was 8.81 ft and for the minor axis (9.84 ft) of the target, the resulting rms miss distance was found to be 1.64 feet.

The total rms miss-distance due to all three noise sources (i.e. receiver, range independent and glint noise) can be obtained by obtaining the root-sum-squared value and is $\text{rms miss} = ((.45)^2 + (.48)^2 + (8.81)^2)^{\frac{1}{2}} = 8.83$ ft for the major target dimension and $\text{rms miss} = ((.45)^2 + (.48)^2 + (2.64)^2)^{\frac{1}{2}} = 2.72$ ft for the minor target dimension. Due to the ratios of the glint miss to receiver or independent miss, the resultant total rms miss is essentially the miss distance due to the glint noise.

Not taken into account in the above noise models has been the degree of correlation of the error or the amplitude from one observation to the next. In the actual missile this can be important because it will determine the response of the measurement system as well as the effectiveness of a smoothing filter. Decorrelation may be caused by target rotation relative to the line-of-sight or intentionally created using a frequency diversity system.

To achieve a hit capability of more than or equal to 99.5%, it is required that $\sigma_{miss}^2 \leq (\frac{L}{8})^2$, where L is the target dimension. Thus for a hit capability equal to 99.5%, the rms miss for the target dimension is $(\frac{32.8}{8}) = 5.47$ ft and for the minor target dimension is $(\frac{9.84}{8}) = 1.64$ feet

Since the present miss distance for the weapon is essentially due to glint noise, it can be reduced to the desired values for a PH of 99.5% by either the use of frequency diversity or by increasing the weapon response time. Although increasing the weapon response time will decrease the miss due to glint noise, it will increase the miss distance due to all other sources. The use of frequency diversity is therefore considered to be the preferred method of decreasing the miss distance and has been analyzed below.

The number of independent samples required to achieve a PH = 99.5% is

$$\eta_f = \left(\frac{\text{miss achieved}}{\text{miss desired}} \right)^2 = \left(\frac{2.64}{1.64} \right)^2 \left(\frac{8.81}{5.47} \right)^2 = 2.59 \quad (139)$$

For uniformly distributed scatterers, the correlation frequency interval f_c is given by

$$f_c = \frac{c}{2L} = \frac{3 * 10^8}{2 * 3} = 50 \text{ MHz} \quad (140)$$

where c is the speed of light and L the minor target dimension in meters. The required bandwidth Δf can be determined from

$$\Delta f = (n_f - 1)f_c = 1.59 * 50 = 80 \text{ MHz} \quad (141)$$

which is .04% of the 200 GHz radar.

Miss distances versus time-to-go, due to transient type causes are shown in Fig. 7 for an initial heading error of one degree, a filtered step acceleration of 32.2 feet/sec² through a 2 second time constant, a sinusoidal target acceleration of 32.2 feet/sec² at a frequency of -5 rad/sec and of a step target displacement of 100 feet. It is clear from the figure that a step target acceleration just before intercept or at times-to-go of .65 and 1.7 seconds will result in the maximum benefit to the target. On the other hand, any maneuvers before a time-to-go of three seconds and at .28 and 1.15 seconds to go are of no benefit to the target.

3.8 Navigation Law Implementation

Implementation of the navigation laws will be relatively simple using the on-board available sensors plus an extended Kalman filter for the terminal navigation law, to estimate target motion and time-to-go. Because the measurements from the sensor are in the sensor's coordinate system, the body motion sensors are in the vehicle's body fixed coordinate system, and the navigation commands to the autopilot have to be in the vehicle's body fixed coordinate system, it is necessary to implement transformation matrices relating the sensor's coordinate system to the vehicle's body fixed coordinate system to the inertial coordinate system. Since all those equations, including the Kalman filter and navigation laws, are quite readily expressed in terms of vectors and matrices, and

since their calculations are naturally performed by matrix manipulations, it becomes rather attractive to provide the navigation computer with an interpreter that translates a powerful convenient set of matrix and vector instructions into machine language at the time of machine execution of each instruction. If all those computations were programmed as scalar equations, a great deal of storage for programs would be required and a great deal of the elegance of the equations would be lost. On the other hand, an interpreter requires some storage and could increase the execution time of the navigation computations, which in turn can affect the accuracy and stability of the navigation and control loop.

When the rocket engine is throttleable, there is a certain amount of latitude in the choice of *Tgo* because there is then additional flexibility in the allocation of thrust acceleration. The navigation solutions determine the required allocation of thrust acceleration along each coordinate axis. Since the component of thrust acceleration along any axis is obtained from a single thrust acceleration vector, the total thrust acceleration must be time-shared among the controlled axes. The program for time-sharing this thrust acceleration must be carefully planned so that the solutions to the problems along the controlled axes are realized simultaneously.

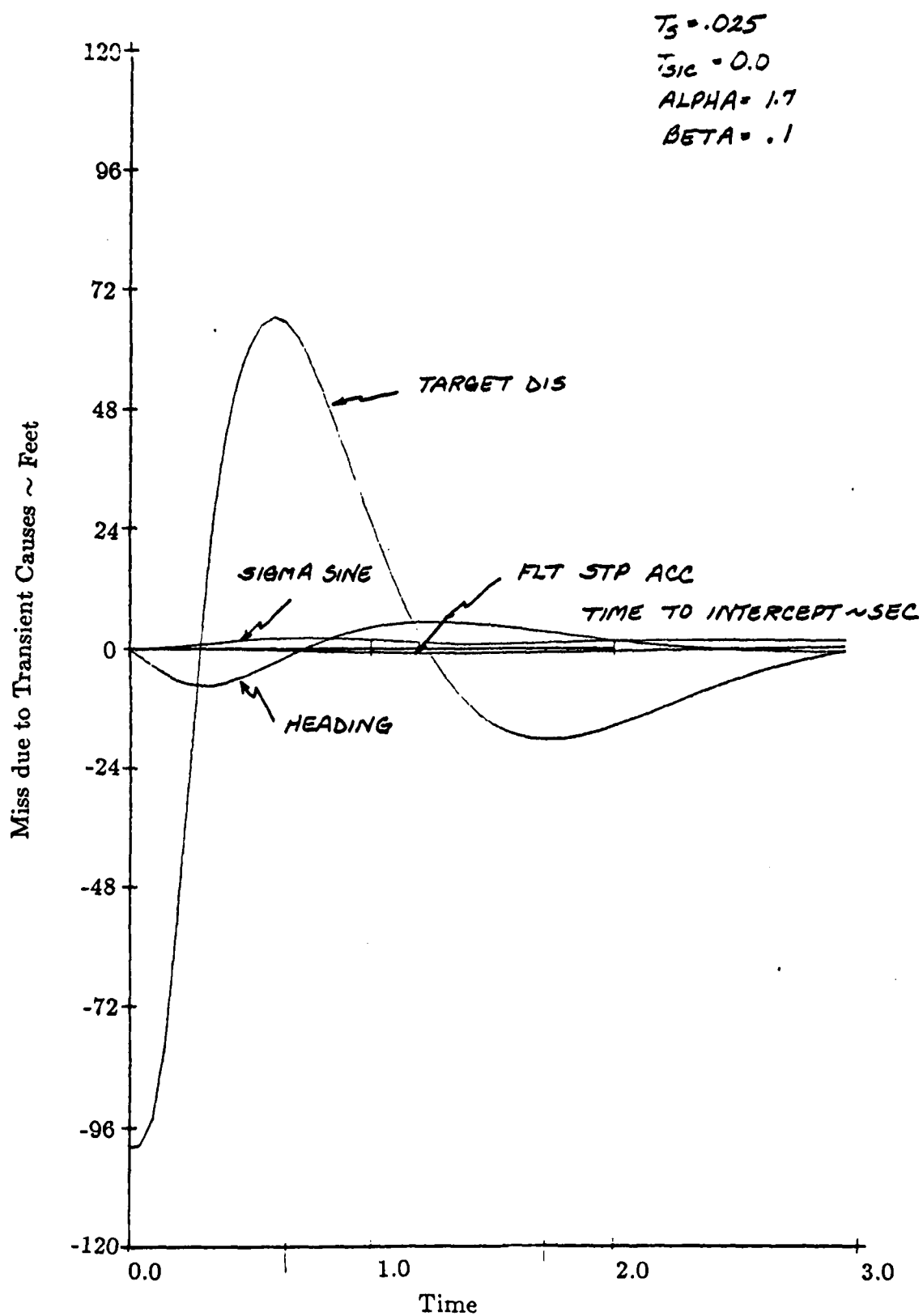


Fig. 7: Miss due to Transient Type Cause for a Sampling Rate of 40 cps

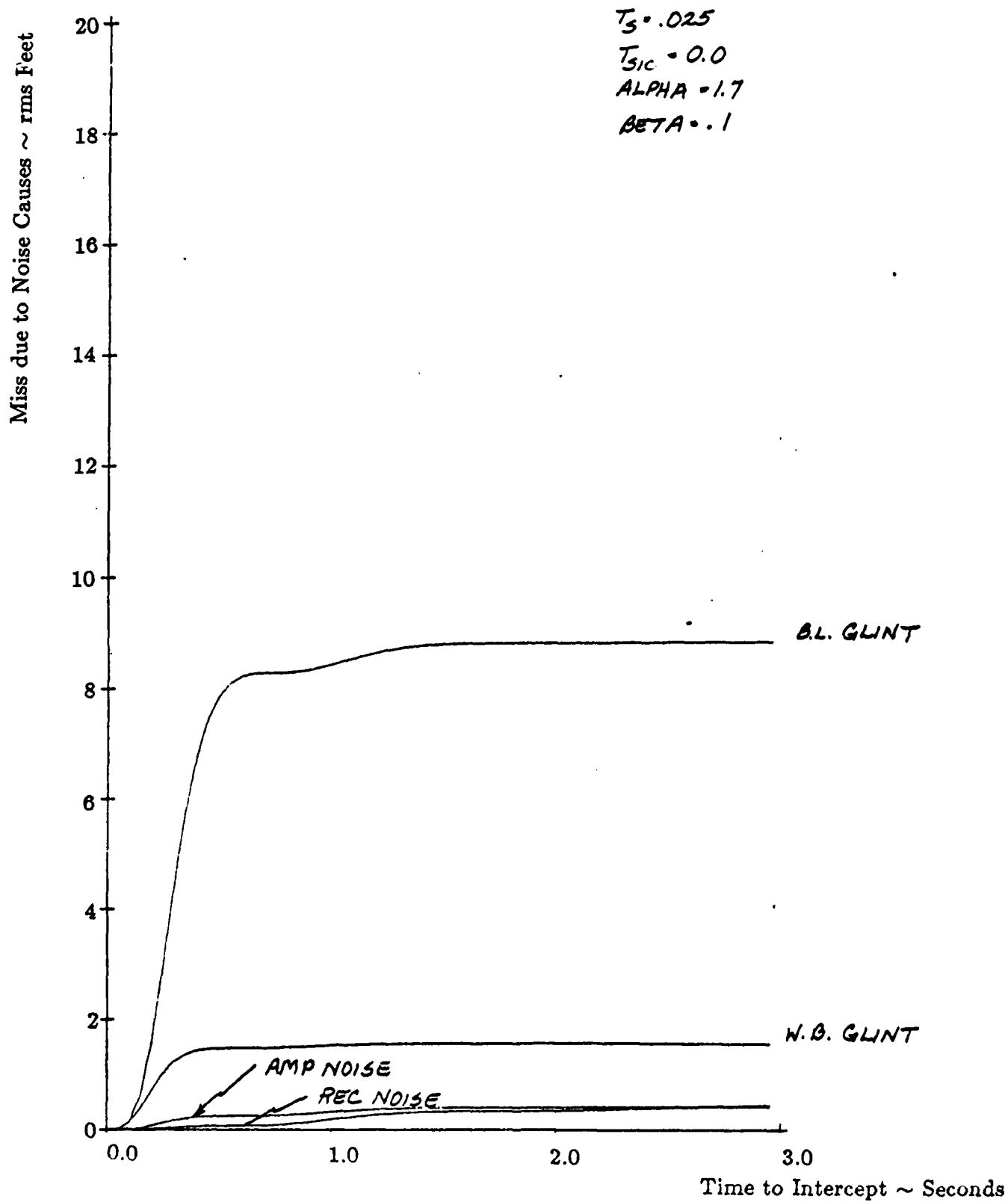


Fig. 8: Miss due to Noise Causes for a Sampling Rate of 40 cps

4.0 Conclusions

The navigation laws developed in this report can control final coordinates of positions as well as final components of velocity and control throttleable as well as fixed thrust rockets. The steering commands are directly in terms of the current and desired boundary values of the components of the position and velocity vectors. The equations are exact and can accommodate any gravitational field model. By treating the weighting parameters explicitly, universal navigation laws have been obtained that are applicable to many-faceted complex missions.

For applications to the various missions, the weighting parameters should be optimized and unified as much as possible, taking into consideration the actual fuel budgets, fixed or throttleable rockets, vehicle dynamics and other factors, to establish the optimal levels of control for those missions. The most economical and effective method to evaluate the algorithms for any mission is to implement a detailed simulation of the system and to perform simulated fly-outs against maneuvering and non-maneuvering targets.

Such a simulation could consist of a six-degree-of-freedom model of the system, containing detailed math models of the major subsystems, including the sensor, autopilot and propulsion, detailed aerodynamic models of the airframe characteristics supported by wind tunnel generated aero data, and the models that describe the vehicle's equation of motion. In addition, the simulation could contain a three-degree-of-freedom target model that incorporates a suitable evasive maneuver algorithm. To obtain actual system performance the transfer alignment errors at initialization and the instrument drifts during flight need to be implemented. They will affect the size of the error basket at handover to terminal navigation. Once in the terminal navigation mode, those errors are of no further concern.

For the terminal navigation law using a terminal sensor, an extended Kalman filter, which is typically based upon the same equations of motion as used for the terminal navigation law, should be developed and implemented in the simulation. In addition, this filter should also be used to obtain an estimate of time-to-go. During the development of the Kalman filter it will also be necessary to investigate in which coordinate reference frame (sensor, body, or inertial) the Kalman filter should be implemented.

Mechanization of the navigation laws and Kalman filter, together with the coordinate reference transformations, should then be implemented and evaluated on the simulation which will lead to the navigation/estimation mechanization specifications for the navigation computer.

BIBLIOGRAPHY

- B. Mons, "Differential Games with Noise Corrupted Measurements", *J. Optimization Theory Appl.*, 28, No. 3 (1978).
- B. Mons, "On-Line Solution of a Stochastic Pursuit - Evasion Game", *J. Optimization Theory Appl.*, 28, No. 4 (1979).
- B. Mons, "Stochastic Differential Game Techniques", in *Control and Dynamic Systems*, Vol 17, Academic Press, 1981. Edited by C.T. Leondes.

LIST OF SYMBOLS AND ABBREVIATIONS

H	- Hamiltonian
J	- performance criterion/optimal control trajectory
L	- minor target dimension in meters
M	- missile position vector
T	- time to orbit
a	- acceleration
c	- speed of light
g	- gravitational force
h	- constant specific angular momentum of the orbit
r	- position vector from the center of the earth
u	- control vector of acceleration
v	- velocity vector
z	- state/costate vector
$u_i^o(t)$	- continuous optimal feedback control terms
Φ	- transition matrix
Ψ	- angle between r and an arbitrary reference
δf	- bandwidth
λ	- costate vector of the Lagrange multiplier
μ	- constant, defining the specific gravitational force
τ	- true line-of-sight angle
τ'	- apparent line-of-sight angle
$\dot{\tau}'$	- rotation rate of apparent line-of-sight angle
IRU	- Inertial Reference Unit
BIM	- Ballistic Intercept Missile
INS	- Inertial Navigation System
T_{go}	- Time-to-go
FOV	- Field of view

INDEX

Adjoint simulation	4, 35, A2
Autopilot	30, 33
Boresight error	23, 30, 32, 33, 34, 35, 37
Differential equations of motion	3, 5, 6
Guidance computer	7
Hamiltonian	7, 11, 14, 25
Inertial reference frame	1, 30
Inertial reference system	5
Inertial reference unit	3
Kalman filter	1, 38, 42
Midcourse guidance	2
Midcourse navigation law	23
Mission Requirements	3
Optimal acceleration	13
Optimal control theory	2, 5, 6, 7, 24
Optimal midcourse navigation policy	1, 5
Performance index	3, 7, 14
Quasi-analytical solution	3, 6, 8
Statistical disturbances	5
Terminal boundary condition	6
Terminal guidance	2
Terminal homing	2
Terminal navigation law	1, 23, 36, 38, 42
Thrust acceleration	1
Two-point boundary value problem	2, 3, 6, 8

APPENDIX A

ADJOINT METHOD OF ANALYSIS

The adjoint method of analysis has proven to be a very useful concept for studying the effects of forcing functions and initial conditions on linear combinations of the state variables of the original system.

If the original time-varying system can be described by the vector-matrix equation:

$$\dot{\mathbf{x}}(t) = \mathbf{A}(t)\mathbf{x}(t) \quad \text{A-1}$$

then the corresponding adjoint system is defined by

$$\dot{\boldsymbol{\alpha}}(t) = -\mathbf{A}^T(t)\boldsymbol{\alpha}(t) \quad \text{A-2}$$

The solution of the original system is given by

$$\mathbf{x}(t) = \boldsymbol{\Phi}(t, \tau)\mathbf{x}(\tau) \quad \text{A-3}$$

where $\boldsymbol{\Phi}(t, \tau)$ is the state transition matrix and satisfies

$$\dot{\boldsymbol{\Phi}}(t, \tau) = \mathbf{A}(t)\boldsymbol{\Phi}(t, \tau), \quad \boldsymbol{\Phi}(\tau, \tau) = \mathbf{I} \quad \text{A-4.}$$

Similarly, the solution to the adjoint system is given by

$$\boldsymbol{\alpha}(t) = \boldsymbol{\Psi}(t, \tau)\boldsymbol{\alpha}(\tau) \quad \text{A-5}$$

where $\boldsymbol{\Psi}(t, \tau)$ is the state transition matrix and satisfies

$$\dot{\boldsymbol{\Psi}}(t, \tau) = -\mathbf{A}^T(t)\boldsymbol{\Psi}(t, \tau), \quad \boldsymbol{\Psi}(\tau, \tau) = \mathbf{I} \quad \text{A-6}$$

The state transition matrix for a time-varying system has two variables, one being the application of the cause, and the

other the time of observation of the effect. The usefulness of the adjoint system stems from the fact that

$$\psi^T(t, \tau) = [\phi(t, \tau)]^{-1} \quad \text{A-7}$$

or

$$\psi^T(t, \tau) = \phi(\tau, t) \quad \text{A-8}$$

Thus the behavior of the system with respect to the variable t is a function of the dynamics of the original system while the behavior of the system with respect to the second variable τ is a function of the dynamics of the adjoint system.

The vector-matrix equation for a system with input $u(t)$ and output $y(t)$ is given by

$$\dot{x}(t) = A(t)x(t) + B(t)u(t) \quad \text{A-9}$$

$$y(t) = C(t)x(t) \quad \text{A-10}$$

where $A(t)$ is an $n \times n$ system matrix

$B(t)$ is an $n \times m$ input matrix

$C(t)$ is a $p \times n$ output matrix

and the system has m inputs $u(t)$ and p outputs $y(t)$.

The general solution to the above system is given by

$$x(t) = \phi(t, \tau)x(\tau) + \int_{\tau}^t \phi(t, v)B(v)u(v)dv \quad \text{A-11}$$

$$y(t) = C(t)\phi(t, \tau)x(\tau) + \int_{\tau}^t C(t)\phi(t, v)B(v)u(v)dv \quad \text{A-12}$$

where $\phi(t, \tau)$ is as before the state transition matrix of the homogeneous equation $\dot{x}(t) = A(t)x(t)$ and satisfies

$$\dot{\phi}(t, \tau) = A(t)\phi(t, \tau), \quad \phi(\tau, \tau) = I \quad \text{A-13}$$

The adjoint system corresponding to the original time-varying system is again given by

$$\dot{\alpha}(t) = -A^T(t)\alpha(t) \quad \text{A-14}$$

whose solution is given by

$$\alpha(t) = \psi(t, \tau)\alpha(\tau) \quad \text{A-15}$$

where $\psi(t, \tau)$ satisfies as before

$$\dot{\psi}(t, \tau) = -A^T(t) \psi(t, \tau) \quad A-16$$

Taking the inner product of the original system solution (A-11) with the adjoint solution (A-15) gives

$$\alpha^T(t)x(t) = \alpha^T(\tau)\psi^T(t, \tau)\phi(t, \tau)x(\tau) + \int_{\tau}^t \alpha^T(v)\psi^T(t, v)\phi(t, v)B(v)u(v)dv \quad A-17$$

or after using A-8

$$\alpha^T(t)x(t) = \alpha^T(\tau)x(\tau) + \int_{\tau}^t \alpha^T(v)B(v)u(v)dv \quad A-18$$

For a fixed terminal time T and for $\tau = -\infty$

$$\alpha^T(T)x(T) = \int_{-\infty}^T \alpha^T(v)B(v)u(v)dv \quad A-19$$

since $\alpha(-\infty) = 0$.

Equation A-19 can now be used to determine the linear combinations of the state variables, $x_1(t)$'s, once the adjoint equation has been solved for the $\alpha(v)$'s.

In the time-varying case this generally must be done by simulation because of the difficulty in analytically solving time-variable differential equations.

Solution of A-19 requires specification of the boundary conditions on $\alpha(v)$. The boundary conditions which should be specified depend upon the problem to be solved. For example, if the effect of the forcing functions and/or initial conditions on $x_1(t)$ is to be determined, the appropriate boundary conditions are $\alpha_1(t) = \delta$ and $\alpha_2(t) = \alpha_3(t) = \dots \alpha_n(t) = 0$.

where δ is the Kronecker delta or unit impulse. Thus a judicious selection of the terminal constraint can easily result in A-19 containing $\alpha_1(T)x_1(T)$ as the only component at time T .

If $\alpha(T)$ is chosen as

$$\alpha^T(T) = [C_{11}(T) \ C_{12}(T) \ C_{13}(T) \ \dots \ C_{1n}(T)] \quad A-20$$

where the C_{ij} 's are the i th row elements of the $p \times n$ output matrix C at terminal time T , then the output

$$y_1(T) = [C_{11}(T) \ C_{12}(T) \ \dots \ C_{1n}(T)] x(T) \quad A-21$$

can be obtained, or

$$y_1(T) = \int_{-\infty}^T \alpha^T(v) B(v) u(v) dv \quad A-22$$

In order to make these boundary conditions initial conditions in the simulation let $v = T - \tau_1$ or $\tau_1 = T - v$.

Since v runs "forward in time" from $-\infty$ to T , τ_1 runs "backward in time" from $\tau_1 = 0$ to $\tau_1 = \infty$, thus

$$y_1(T) = - \int_0^{\infty} \alpha^T(T-\tau_1) B(T-\tau_1) u(T-\tau_1) d\tau_1 \quad A-23$$

and the corresponding adjoint system is

$$\frac{d\alpha(T-\tau_1)}{d\tau_1} = A^T(T-\tau_1) \alpha(T-\tau_1) \quad A-24$$

The coefficient matrix of this equation is the transposed A matrix of the original system, with t replaced by $T - \tau_1$. The initial conditions for this system are then

$$\alpha^T(0) = [C_{11}(T), \ C_{12}(T) \ \dots \ C_{1n}(T)] \quad A-25$$

Those initial conditions can be established by applying a unit impulse at $\tau_1 = 0$ through gains of

$$\begin{array}{l} C_{11} (T - \tau_1) \\ C_{12} (T - \tau_1) \\ C_{13} (T - \tau_1) \\ . \\ . \\ C_{in} (T - \tau_1) \end{array} \quad A-26$$

Since B and C are, respectively, the input and output matrices of the original system, the net result is that the ith row of

$$\int_0^{\infty} \alpha(T-\tau_1) B(T-\tau_1) u(T-\tau_1) d\tau_1 \quad A-27$$

is generated for variable τ by reversing the input and output of each of the simulation elements of

$$\dot{x} = A(t)x + B(t)v \quad A-28$$

$$y = C(t)x$$

and replacing the time t of any time-varying gains by $T - \tau_1$. If the original system has m inputs and p outputs, the adjoint system has p inputs and m outputs. Each simulation run of the adjoint simulation produces m outputs. These m outputs comprise a row of C where the running variable of simulation time is τ . The particular row of the matrix is determined by the input on which the unit impulse is placed at the beginning of the simulation run.

For example, if the unit impulse is placed on the state variable that represents miss distance in the forward simulation, the outputs of the adjoint simulation represent the miss distance caused by the corresponding input variable of the forward simulation.

Starting with a block diagram representation of the forward system, construction of the adjoint simulation takes place by

1. Reversing all signal flows
2. Redefining branch points as summing blocks
3. Redefining summing blocks as branch points
4. Replacing t by $T - \tau_1$ in the arguments of all time-varying coefficients.

APPENDIX B ADJOINT SIMULATION

In order to generate the adjoint simulation it was first necessary to develop a block diagram of the forward simulation after which the adjoint simulation could be developed using the rules stated in Appendix A, i.e.

1. Reverse all signal flows
2. Redefine branch points as summing blocks
3. Redefine summing blocks as branch points
4. Replace t by $T - \tau_1$ in the arguments of all time-varying coefficients.

The space diagram showing the geometric relationship between the missile and target is shown in Figure B-1. The missile and target velocity, V_m and V_t respectively, are assumed to be constant

Gravity effects are neglected and the encounter is assumed to be restricted to the x-y plane. The angles are, of course, subject to change because both missile and target are free to maneuver in the x-y plane.

The fundamental relations governing the missile and target paths during the terminal engagement are the following velocity

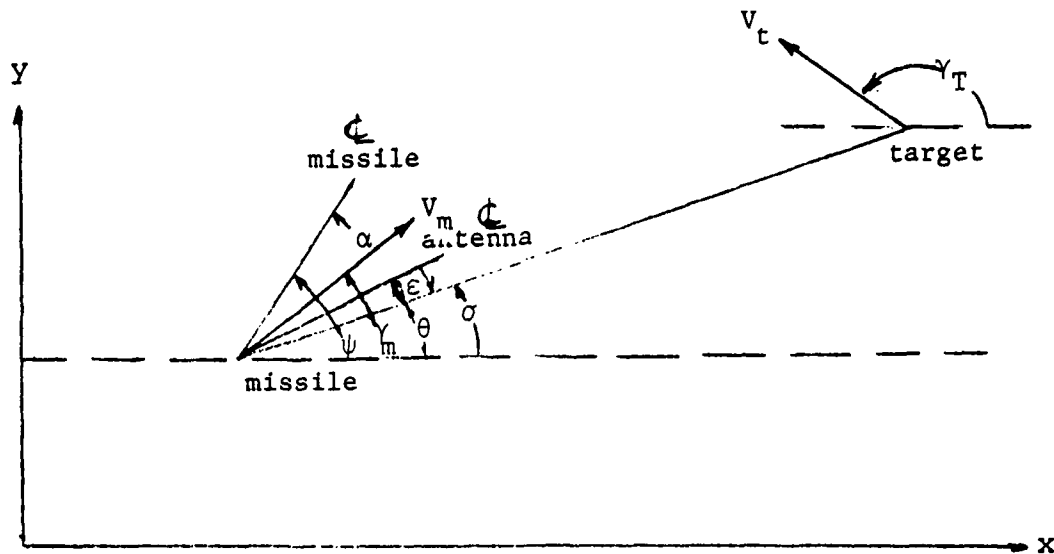


Fig. B-1: Space Diagram for a Homing Missile

equations:

$$y_t = V_t \sin \gamma_T \quad \text{B-1}$$

$$y_m = V_m \sin \gamma_M \quad \text{B-2}$$

$$x_t = V_t \cos \gamma_M \quad \text{B-3}$$

$$x_t = V_t \cos \gamma_T \quad \text{B-4}$$

The angles γ_M and γ_T start at $t = 0$ from some initial values γ_{T0} and γ_{M0} and are perturbed by small amounts γ_m and γ_t during the encounter. Under these conditions, the instantaneous angles of the velocity vectors are

$$\gamma_M = \gamma_{M0} + \gamma_m \text{ and } \gamma_T = \gamma_{T0} + \gamma_t \quad \text{B-5}$$

so that the linear velocity components are

$$y_t = V_t \sin(\gamma_{T0} + \gamma_t) \approx V_t \sin \gamma_{T0} + \gamma_t V_t \cos \gamma_{T0} \quad \text{B-6}$$

$$y_m = V_m \sin(\gamma_{M0} + \gamma_m) \approx V_m \sin \gamma_{M0} + \gamma_m V_m \cos \gamma_{M0} \quad \text{B-7}$$

$$x_t = V_t \cos(\gamma_{T0} + \gamma_t) \approx V_t \cos \gamma_{T0} - \gamma_t V_t \sin \gamma_{T0} \quad \text{B-8}$$

$$x_m = V_m \cos(\gamma_{M0} + \gamma_m) \approx V_m \cos \gamma_{M0} - \gamma_m V_m \sin \gamma_{M0} \quad \text{B-9}$$

where the small angle approximations $\sin \gamma = \gamma$ and $\cos \gamma = 1$ have been used.

If we assume that the missile and target are initially on a lead collision course, $\gamma = 0$ and

$$V_t \sin \gamma_{T0} = V_m \sin \gamma_{M0} \quad \text{B-10}$$

and the projected miss rate M_y is given by

$$M_y = y_t - y_m \approx \gamma_t V_t \cos \gamma_{M0} - \gamma_m V_m \cos \gamma_{M0} \quad \text{B-11}$$

Using (B-8), (B-9) and (B-10) we have

$$x_t - x_m \approx (V_t \cos \gamma_{T0} - V_m \cos \gamma_{M0}) - (\gamma_t - \gamma_m) V_m \sin \gamma_{M0} \quad \text{B-12}$$

If we neglect the difference term in B-12 involving $\gamma_t - \gamma_m$, the closing rate V_c is given approximately by

$$-V_c \approx x_t - x_m \approx V_t \cos \gamma_{T0} - V_m \cos \gamma_{M0} \quad \text{B-13}$$

and the missile-to-target range $R(t)$ is

$$R(t) \approx R_0 - V_c t \quad \text{B-14}$$

The target bearing as viewed by the missile homing system is σ , where

$$\sigma \approx \frac{M_y}{R(t)} = \frac{1}{R(t)} \int_0^t \dot{M}_y dt.$$

B-15

A block diagram representative of the linearized kinematics for a homing missile is shown in Figure B-2.

The kinematics represent that portion of the problem that one must live with, i.e. those are the elements of the problem about which one has no choice, and which must be accepted the way they are.

The system must then operate on the sight angle σ in such a way that the final value of M_y (when $t = R_0/V_c$ or $x_t = x_m$) is made as small as possible.

Two observations can be made at this point. First, a double integration appears in that portion of the kinematic loop of

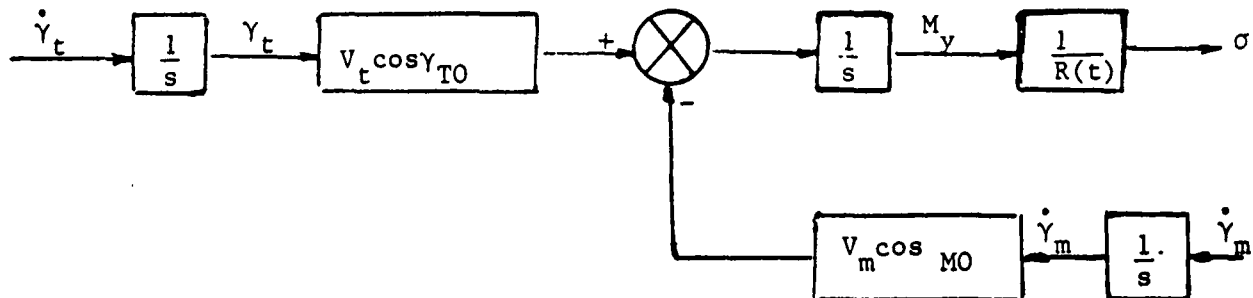


Fig. B-2: Linearized Homing Missile Kinematics

Figure B-2 joining $\dot{\gamma}_m$ to σ . Consequently, the control portion of the loop, whatever it may be, must necessarily provide some derivative effect if system stability is to be insured. Secondly, since the kinematic loop possesses a time dependent division by range $R(t)$, a linear time-varying system results even if γ_m and σ are coupled by a constant coefficient control.

A practical method of control that has received widespread application, and which is used in the HAWK missile, is proportional navigation. In this type of control one tries to make the missile-path turning rate proportional to the line-of-sight rate. It is clear that if the angular rotation of the line-of-sight between missile and target can be made to vanish and the range rate is of such a sign as to result in closure, collision is inevitable. Of course, the line-of-sight rate cannot be reduced to zero and held there in any practical system because of a number of system imperfections, which lead to uncertainty in the true target bearing.

The true miss distance M_T can be defined as

$$M_T = \text{Min} \sqrt{(x_t - x_m)^2 + (y_t - y_m)^2} \quad \text{B-16}$$

which is essentially the distance of closest approach between the missile and target. The radical in B-16 is also the instantaneous range between the missile and target. In our linearized version of the missile system we have chosen the coordinate system in such a way that the approximation equations give

$$\begin{aligned} x_t - x_m &= R_0, & t &= 0 \\ x_t - x_m &= 0, & t &= \frac{R_0}{V_c} \end{aligned} \quad \text{B-17}$$

and used instead the projected miss distance M defined by

$$M_y = y_t - y_m, \quad 0 \leq t \leq R_0/V_c \quad \text{B-18}$$

The forward missile simulation is shown in Figure B-3. The system operates on the sight line angle σ , derived from M_y through division by range $X_{MT} = (x_t - x_m)$, in such a way that the final value of M_y (when $t = R_0/V_c$ or $x_t = x_m$) is made as small as possible.

The HAWK navigation system is implemented with a space-stabilized radar seeker aboard the missile, whose antenna provides a measure of the target bearing σ . Referring to Figure B-1, the centerline of the seeker antenna makes an angle θ with the reference. The angular error in target bearing is

$$\epsilon = \sigma - \theta \quad \text{B-19}$$

The angular error is converted to a voltage by the radar and filtered to provide the necessary driving signal to process the seeker antenna in such a direction as to try continually to reduce the angular error to zero. The filtered drive signal is accordingly

$$E = \frac{k\epsilon}{1 + \tau s} \quad \text{B-20}$$

where a simple, time-constant lag-filter has been used. The precession rate of the seeker θ is proportional to E , so that

$$\theta = kE \quad \text{B-21}$$

where k is the precession constant for the seeker.

The same drive signal E is used as input to the guidance computer where the proportional guidance law and a first order noise filter are implemented. The output of the guidance computer is the normal acceleration command to the autopilot which can be implemented in the simulation as a first, second or third order system.

The output of the autopilot is the missile's normal acceleration in g 's which upon multiplication by $32.2/V_m$ results in the missile velocity vector rotation rate $\dot{\gamma}_m$ in rad/sec. Angle of attack α is proportional to $\dot{\gamma}_m$, i.e. $\alpha = k_\alpha \dot{\gamma}_m$, where k is the inverse of the effective lift coefficient A . The control portion of the missile homing system is completed by integrating the missile velocity vector rotation rate. Thus γ_m together with possible target maneuvers are input to the homing kinematics loop whose output after division by XMT forms the input to the forward simulation.

Boresight error slope is implemented by forming $\sigma - \psi$ and subtracting that signal from σ after multiplication by $k_{ye} = -r$, thus creating

$$\sigma' = \sigma + r(\sigma - \psi) = (1 + r)\sigma - r\psi \quad \text{B-22}$$

The output quantity of interest is M_y , the projected miss distance. XMT is the range at any time t after the start of the homing.

The initial geometry is fixed by the missile and target heading at the start of the homing.

The glint or scintillation noise input is represented as a linear displacement at the target and, like miss distance, is divided by range to become an angular noise input to the seeker. To allow target glint representation as stationary band-limited noise with amplitude and bandwidth dictated by the physical dimensions and motion of the target, a band-limited glint noise input is provided. Since the statistical properties of band-limited noise is the same as filtered "white" noise, a simple lag filter between the band-limited input and the driving white noise is required. The amplitude or fading noise is introduced as an angular uncertainty on σ' and is assumed to be white. Semi-active receiver noise is introduced at the same place after multiplication by XMT squared.

Consider now the initial condition inputs to the system indicated by double arrows in Figure B-3. One such input is the head pointing error at the start of homing and is assumed to be a constant random variable. The initial turning rate and heading error of the missile is shown as an input to $\dot{\gamma}_m$ and γ_m respectively. Either of these errors could be zero under certain circumstances. If the seeker is locked-on and settled out at start of homing, the seeker initial error input becomes zero. If the missile is not maneuvering at the start of homing, the initial turning rate and heading error also vanish. Target maneuvering inputs consisting of step, filtered step and sinusoidal target maneuvers are also shown on Figure B-3.

The forward simulation has 12 inputs and a single output, miss distance. The system adjoint must, therefore, have a single

FORWARD SIMULATION

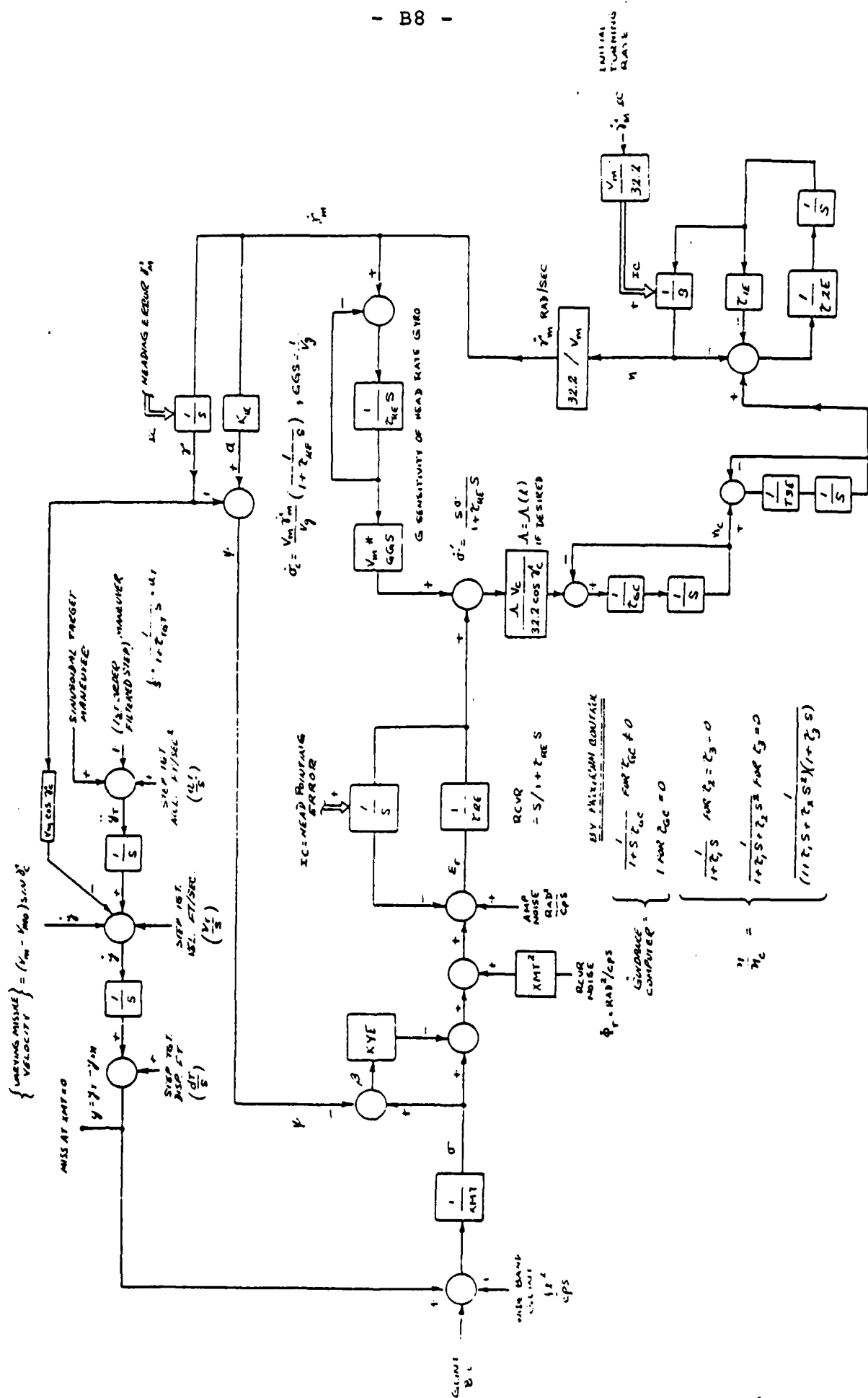


Figure B-3: Forward Missile Simulation

input and 12 outputs. The adjoint is generated by reversing all inputs and outputs and generating all time functions backwards. The adjoint missile simulation is shown in Figure B-4. It has a single impulse input, indicated by the double arrow in Figure B-4, at the point where the miss distance was measured in the forward simulation of Figure B-3. It has 12 outputs, taken from points where the inputs were previously applied. This is indicated in Figure B-4 with M name, where M stands for "miss due to" and name indicates the source causing the miss.

The influence of target maneuvers and initial conditions on miss distance is obtained directly after scaling at the appropriate outputs of the adjoint simulation. The influence of noise disturbances on miss is obtained by first squaring the output, then scaling and taking the integral of the squared output. In order to obtain the rms miss distance the square root is then taken. Thus for the rms miss distance due to glint noise obtained at A1 in Figure B-4, the output is first squared and then integrated and scaled, after which the square root is taken.

Thus a single run of the adjoint simulation provides the effects on missile miss distance of each of the input quantities, such as target maneuvers, initial conditions and statistical disturbances, so that one may see which factors are the most important. This represents a tremendous saving in time over Monte Carlo techniques (repeated simulation trials plus ensemble averaging).

2D ADJOINT SIMULATION

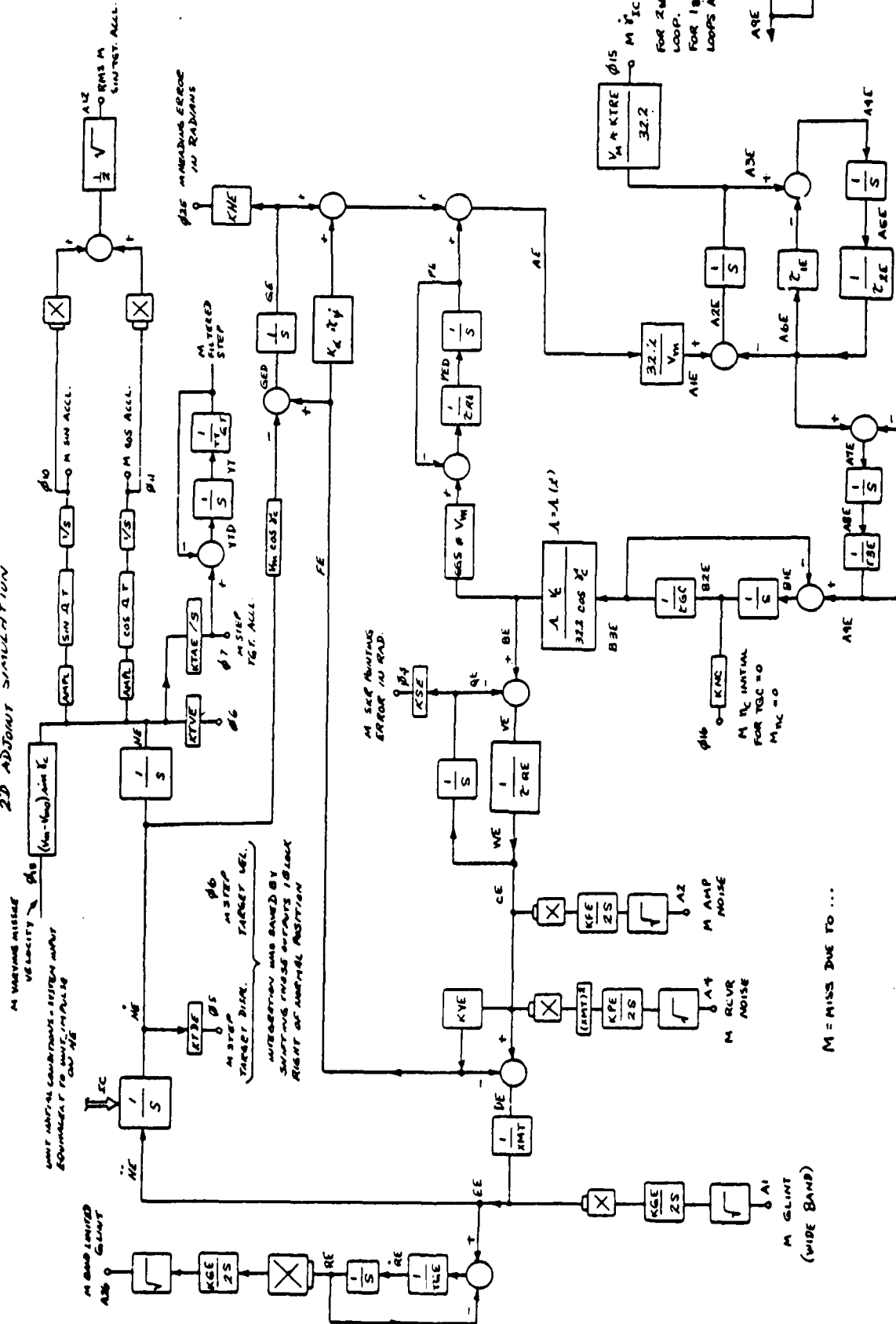


Figure B-4: Adjoint Missile Simulation